Study the effect of liquid impingement corrosion/erosion with and without solid particles on two pipeline grades API X65 and Mild Steel AISI 1030

BY

Hafiz Muzammil Irshad

A Thesis Presented to the

DEANSHIP OF GRADUATE STUDIES

KING FAHD UNIVERSITY OF PETROLEUM & MINERALS

DHAHRAN, SAUDI ARABIA

In Partial Fulfillment of the
Requirements for the Degree of

MASTER OF SCIENCE

In

Materials Science and Engineering

April 2017

KING FAHD UNIVERSITY OF PETROLEUM & MINERALS

DHAHRAN- 31261, SAUDI ARABIA

DEANSHIP OF GRADUATE STUDIES

This thesis, written by **Hafiz Muzammil Irshad** under the direction his thesis advisor and approved by his thesis committee, has been presented and accepted by the Dean of Graduate Studies, in partial fulfillment of the requirements for the degree of **MASTER OF SCIENCE IN MATERIALS SCIENCE & ENGINEERING.**

Dr. Ihsan ul Haq Toor
(Advisor)

Dr. Zuhair Mattoug Gasem
Department Chairman

Dr. Hassan M. Badr
(Member)

Dr. Salam A. Zummo
Dean of Graduate Studies

Dr. Abdul Samad Mohammad
(Member)

3/5/17
Date

This is dedicated to my grandmother and beloved parents.

ACKNOWLEDGMENTS

I express my gratitude and praise to ALMIGHTY ALLAH, the creator of universe, who is beneficial and merciful, guided us in difficult and congeal circumstance, who endowed us with the will to complete this project. Great respect to our Holy Prophet Hazrat Muhammad (PBUH), who taught us to learn till cradle to grave.

I would like to thank my advisor Dr. Ihsan ul Haq Toor for his support and encouraging me to uptake this challenge and guiding me till the end of this research. I would like to thank my committee member, Dr. Hassan M. Badr for helping a lot in calculations and making my technical concepts strong in fluid mechanics, provided me material to read and gave his useful comments and suggestions. I am also thankful to Dr. Abdul Samad Mohammad for providing me the laboratory facilities and his valuable input in this thesis work.

I thank to Mr. lateef Hashmi (Lab Engineer), for providing me lab assistance in the lab. Financial support and resources for this research provided by Deanship of Scientific Research (Project No. 141022), and Mechanical Engineering Department.

I am grateful to my friends, especially my roommate Mr. Mohammad umair, Mr. Mohammad Irfan Malik from chemical engineering department, Annas Bin Ali, and Bilal Saghir for making this journey happy and memorable.

Finally, I would like to thank my grandmother, teachers, parents, bother, and sisters in my country who prayed for my success.

TABLE OF CONTENTS

LIST OF TABLES

LIST OF FIGURES

LIST OF ABBREVIATIONS

FE-SEM	:	Filed Emission Scanning Electron Microscope
NaCl	:	Sodium Chloride
IC	:	Impingement Corrosion
IE	:	Impingement Erosion
IEC	:	Impingement Erosion Corrosion
SP	:	Solid Particles
CFD	:	Computational Fluid dynamics
AISI	:	American Institute of Steel and Iron
API	:	American Petroleum Institute
TDS	:	Total Dissolved Salt
ASTM	:	American Standard of Testing Materials
M-NaCl	:	Molar Sodium Chloride
EDX	:	Energy Dispersive X-Ray

ABSTRACT

Full Name : Hafiz Muzammil Irshad

Thesis Title : Study The Effect Of Liquid Impingement Corrosion/Erosion With and Without Solid Particles On Two Pipeline Grades API X65 & Mild Steel AISI 1030

Major Field : Materials Science and Engineering

Date of Degree : April 2017

In this study, the impingement corrosion and erosion-corrosion characteristics of two types of carbon steel alloys due to liquid jet impingement were investigated. The study was focused on the effect of jet velocity and jet angle on the rate of impingement erosion-corrosion with and without the solid particles of size ranging from 125µm-704µm (means size of 314 µm). Fluid impingement on fluid handling equipments at high velocities results in severe impingement erosion-corrosion issues in different industries. The impingement erosion-corrosion behavior of carbon steel AISI 1030 and API 5L- X65 was investigated experimentally taking into consideration the effect of velocity and different impingement angels (e.g. 15°, 30°, 45°, 60°, & 90°) in 0.2M NaCl solution for twenty four hours.

The maximum impingement erosion-corrosion rate was observed at 45° in three different velocities (i.e. 3, 6 & 12 m/s). This maximum erosion-corrosion rate is resulted to the combined effect of shear stress and impact stress on the specimen surface during the test. At lower angles (15°-30°) shear stress was dominant and at higher angles (60°-90°) normal impact stress was dominant. However, there was a balance between these two stresses at 45°, which resulted in the peak impingement erosion-corrosion rate with the

deepest wear scar (57μm deep). The wear scar depth in high velocity regions, (near impingement zone) was visualized by optical profilometer. It was observed that with an increase in velocity, the impingement erosion-corrosion rate was also increased.

Impingement erosion-corrosion mechanism was analyzed using SEM of the eroded surfaces. Observations of the SEM micrographs, demonstrated that, the recessed scars were formed in the direction of fluid flow. At lower angles (15º-30º) the shallow-elongated ploughing, plastic deformation, raised lips followed by flattening of the ridges were observed. Whereas, at intermediate angles, deep ploughing and deep craters were found. However dimples, micro-forging, extrusion, platelet formation and their removal were identified as dominant mechanisms at 90° angle in the impingement erosion-corrosion experiments.

ملخص الرسالة

الاسم الكامل : حافظ مزمل إرشاد

عنوان الرسالة : دراسة تأثير التعرية السائلة للتآكل / التآكل مع وبدون جزيئات صلبة على درجتي خطوط الأنابيب أبي 65X والفولاذ الطري إيسي 1030

التخصص : علم و هندسة المواد

تاريخ الدرجة العلمية : أبريل 2017

في هذه الدراسة، تم التحقق من خصائص مقاومة التآكل والتآكل من نوعين من سبائك الصلب الكربوني بسبب الاصطدام النفاث السائل. وركزت الدراسة على تأثير سرعة النفاثة وزاوية النفاثة على معدل الاصطدام بالتعرية التآكل مع وبدون الجسيمات الصلبة التي تتراوح من mμ125-mμ704 (يعني حجم 314 ميكرون). ويؤدي اصطدام السوائل على معدات معالجة السوائل بسرعات عالية إلى حدوث مشاكل شديدة في التآكل والتآكل في الصناعات المختلفة. تم دراسة سلوك التعرية التآكل من الكربون الصلب إيسي 1030 و أبي 65X -L5 تجريبيا مع الأخذ بعين الاعتبار تأثير السرعة ومختلف الملائكة الاصطدام (على سبيل المثال° 15 ،° 30 ،° 45 ،° 60 ، و° 90 درجة) في M 0.2 كلوريد الصوديوم حل لمدة أربع وعشرين ساعة.

لوحظ أن الحد الأقصى للتآكل في معدل التآكل عند 45 درجة في ثلاث سرعات مختلفة (أي 3 و 6 و 12 م / ث). ويؤدي هذا الحد الأقصى للتآكل معدل التآكل إلى التأثير المشترك للإجهاد القص والإجهاد تأثير على سطح العينة أثناء الاختبار. في الزوايا السفلية (° 15 - ° 30) كان إجهاد القص مهيمنا، وفي زوايا أعلى (° 60 ° -90 درجة) كان التأثير الطبيعي للإجهاد سائدا. ومع ذلك، كان هناك توازن بين هذين الإجهادين في 45 درجة، مما أدى إلى الذروة الانكماش معدل التآكل مع أعمق ندبة ارتداء (mμ57 عميقة). تم تصور عمق ندبة ارتداء في مناطق سرعة عالية، (بالقرب من منطقة الاصطدام) بروفيلوميتر البصرية. ولوحظ أنه مع زيادة السرعة، ازداد أيضا معدل التعرية للتآكل.

تم تحليل آلية التعرية للتآكل باستخدام تقنية سيم للسطوح المتآكلة. وأظهرت الملاحظات من الميكروسكوب سيم، أن الندوب راحة تشكلت في اتجاه تدفق السوائل. في زوايا أقل (° 15 - ° 30) لوحظ الحراثة الضحلة الممدود، تشوه البلاستيك، رفع الشفاه تليها تسطيح من التلال. بينما، في زوايا وسيطة، تم العثور على الحراثة العميقة والحفر العميقة. ومع ذلك، تم تحديد الثغرات، والتزوير الجزئي، والقذف، وتشكيل الصفائح الدموية وإزالتها كآليات مهيمنة عند زاوية° 90 درجة في تجارب مقاومة التعرية للتآكل.

CHAPTER 1

INTRODUCTION

In modern fluid handling systems, the demands for economical and reliable infrastructure are increasing in all process industrial sectors. The high fluid velocities in combination with corrosive electrolytes and solid particles, result in severe erosion-corrosion of the equipments in different industries. It is a complex phenomenon due to a combined action of electrochemical process of corrosion and mechanical process of erosion. The industries face a loss of billions of Dollars because of erosion-corrosion problem. Erosion-corrosion results in increased maintenance costs, downtime and premature equipment failures [1]. The increased deterioration rates accredited to erosion corrosion problem can produce serious concerns to project economy, operations, where material reliability, long term performance and accurate corrosion rate predictions are the key objectives. Material degradation in the form of corrosion and erosion-corrosion in offshore oil and gas field environments, desalination plants to health care industries has a safety importance to the operators. Damage of facilities by corrosion increases the operation expenditure and the potential costs run into millions of pounds/dollars each year [2][3]. This problem is a common occurrence in fluid handling equipments and ranked as the fifth most important degradation mechanism [4][5].

To fulfill the processing and operational requirements, transportation of fluid or slurry is essential. In many industries, different fluid handling equipments (such as pumps,

compressors, piping systems etc) are in operation for the transportation of aggressive fluids. The fluids that are transported from reservoirs usually have solid particles, which are responsible for the erosion wear damage to the inner surfaces of the equipment. Sand particles are also present in crude oil, associated produced water and also in systems utilizing sea water for cooling purposes. Solid particles have momentum as they come in contact with the surface and hence damage the surface of the fittings, piping system, and pumps. This results in unplanned equipment repair [6]. Similarly Seawater is used in desalination plants, for cooling systems, fire-fighting, and power generating industries, however, in the seawater sand particles can be present, which reduce the design life by a combined effect of erosion-corrosion. By careful simulation of erosion-corrosion one can evaluate high performance materials, conditions, which can be helpful to address the problem of impingement erosion-corrosion. In order to predict the problem effectively, more reliable databases are required. Such reliable data can only be generated, if the lab equipments can simulate the real time situation present in different industries. So therefore, the scope of this work was to develop an in-house reliable erosion-corrosion database for carbon steel. Hence, a state of the art impingement erosion-corrosion Flowloop was developed to perform erosion-corrosion experiments at five different angles, three different velocities, with and with solid particles.

1.1 Flow Accelerated Corrosion

Corrosion that results from the effect of turbulence is defined as flow accelerated corrosion, because of the fluid that does not contain solid particles in adequate quantity and size to impinge on the surface of the metal. The corrosion consists on the transportation of reactants and products to and from the surface. If a reaction on the surface is dependent on the transportation rate of reactants and products. So corrosion will be highly influenced by the flow conditions which could affect its rate. When the flow of fluid is present on the surface, the transportation rate of the reactants and products to and from the surface increases as compared to steady state conditions. This type of increase in corrosion rate is called the flow accelerated corrosion. As the water contact the surface of the target material, in changing turbulence flow condition, flow accelerates the corrosion. Corrosive species reach to the metal surface by fluid flow and removes the corrosion products. Virtually in all conditions where flow accelerated corrosion occurs the flow is turbulent [7]. The regions where flow is disturbed or flow is not in steady state condition, corrosion failures usually occur. Such as:

- Bend elbows
- Inlets of the heat exchanger tubes
- Sites where pits already exist
- At the weld bead sites of downstream
- Tubes of heat exchangers where little blockage occurs.
- Hard shell fouling in down streams
- Valves in downstream
- At threaded joints/ upsets

Fresh corrosives are brought into contact with the surface and corrosion products are swept away, destroying the steady state process. The effect of this flow pattern disruption, or disturbed flow, is the production of a corrosion situation, where the normal steady state corrosion reaction cannot be attained, but instead generates a kinetic disturbed condition. This results in large amount of corrosion at the flow disturbed regions. Corroded areas as large pits or corrosion patterns appears, usually signs of flow directions observed [8].

1.2 Impingement Corrosion

According to ASTM G73-98, Impingement corrosion is a form of erosion corrosion, generally associated with the impingement of a high-velocity jet. The liquid impingement erosion is the progressive loss of original material from a solid surface due to continued exposure to impacts by liquid jets or drops. In a large amount of industrial situations, problems arise when a stream of water impinges on, or flows over, components. The

consequent deterioration process is, exacerbated when the aqueous fluid is corrosive, also fluid flow itself have a role in impingement corrosion or erosion [9][10].

1.3 Slurry Erosion Corrosion

Erosion is derived from the Latin verb “rodene” which means to wear away gradually. It is different from abrasion, where material removal occurs by unidirectional sliding of two bodies. In erosion, solid particles entrained in high velocity jet are repeatedly impacted on the metal at oblique angles, resulting in material removal from the surface, whereas corrosion is a material deterioration process which results because of chemical or electrochemical reactions [11]. However erosion-corrosion caused by flowing fluid in combination of solid particles or absence of solid particles is a form of tribo-corrosion material removal mechanism; damage both the surface layers, (for example passive film or corrosion products) and the base metal. The degradation mechanism is extremely complex and results from the combination of electrochemical and mechanical processes. Mechanisms associated with material loss can vary given that metal can be removed from the surface via chemical dissolution, or erosion caused by fluid flow or the impingement of slurry having solid particles on the surface of the material, and in more intricate processes, electrochemical corrosion can have synergistic effect i.e. it can enhance erosion [12]. As proposed by many researchers [13[[14], the effects of erosion and corrosion in combination can be considerably higher than the sum of the effects of the processes, if they are acting separately.

1.4 Factors Affecting Erosion Corrosion

There are various parameters that effect erosion corrosion such as: angle of impingement, fluid velocity, particle shape, size and concentration, target material, effect of inhibitors etc.

1.4.1 Impingement Angle

There are many factors but one important factor in erosion corrosion is the impingement or impact angle by which the fluid impinges on the target material. Angle between the trajectory of erodent and the surface of the target is defined as the impact angle. Erosion rate dependence on impact angle is detrimental by the type/nature of target material and the fluids that are impinging. Maximum erosion rate in ductile materials such as metals and alloys peaks at low impact angles 15°- 30°.However contrary to it, in brittle material (such as glass) peak erosion rate is usually obtained at normal impact angles i.e. at 90° degrees [15, 16]. Furthermore Matsumura, studied the behavior of pure iron and 304 stainless steel and found that maximum erosion rate peaks from 30° to 50° degree angles and these are eroded by silica sand/water slurry [17]. In the studies of erosion behavior on aluminum by tap-water slurry, similarly Burstein shows that the peak erosion rate appeared at intermediate angles between 40° and 50° degree [18]. However, in literature the dissimilarity of peak erosion rate with impact angle in gas–solid particle erosion is relatively different from the aqueous slurry erosion, that is in airborne particle the peak erosion rate comes around 15°, whereas in aqueous slurry it is around 45°. The inconsistency in the erosion rate as a function of impact angle can stem mainly from the difference in the carrier medium of the particles [19].

1.4.2 Fluid Velocity

Erosion corrosion in many industrial sectors, especially in oil and gas production systems is predominantly due to sand particles impingement. If the particle velocity is increased by the carrier fluid the erosion rate also increased. Higher impact velocity actually increases the kinetic energy of particles and they can penetrate deeper in to the material and enhances the material removal, also fluid velocity affects the flow regime within a pipe section. At lower velocities, flow is mainly laminar and corresponding mass loss is also lower. But, at higher velocities, the flow becomes turbulent and enhances erosion-corrosion. Protective Iron-oxide film is initially broken down by particle impacts and the turbulent flow prevents the re-passivation on the surface of the metal. This results in accelerated material loss from the surface. Hence, as the impingement speed increases it should increase erosion rate [20].

1.4.3 Particle Size and Concentration.

Solid particle size is one of the important factors which affect the erosion rate of material. There is a limit of particle size until which there is an increase in erosion rate that is normally between 100 and 150 μm, after that there is not much increase in erosion rate as in the case of 304 SS eroded with alumina abrasive particles. It is suggested that very small particles cannot enter the hardened layer on the surface as efficiently as larger ones, that could change the erosion mechanism [21]. However it is rarely found that by increasing particle size the erosion rate is decreased and this has been credited to energy loss by particle disintegration. If the particles have individual interaction with the target surface then we can expect linear erosion behavior. However, if the particle concentration

is increased, the increase in the erosion rate does not show a linear correlation with particle concentration. This is due to particle interaction with other particle and particle-surface interactions [22].

1.4.4 Target Material

Rate of erosion corrosion depends on type of target material. Soft metals like aluminum or copper alloys are more susceptible to erosion corrosion. Whereas the alloys that have the ability of passivation are more resistance to erosion corrosion. Addition of alloying elements imparts change in physical properties and can have significant effects on the rate of erosion corrosion e.g. Cr & Mo additions produce improvements to pitting and hence resists against erosion corrosion. However, very hard materials like tungsten carbide could not be eroded even under severe erosion corrosions. Most of the metallic materials eroded in a ductile manner, whereas materials like nickel coated 1018 steel eroded in brittle manner [21].

1.4.5 Effect of Inhibitors

Chemical inhibitor is the most important and common practice to control the erosion corrosion problem especially in mild steels. There are many factors that have influence on the performance of the inhibitors such as inhibitor concentration, type of material, concentration of inhibitor, sand particle concentration, chlorides content, pH of the fluid, velocity of the fluid and others. In some laboratory tests it is shown that inhibitors adsorbed onto the sand particles which are introduced in the fluid, and a larger quantity of inhibitor can be lost from the solution. This decreases the concentration of inhibitor

which should be there to protect steel surface. Whereas such type of effect is prominent in the higher concentration of sand particles and small size particles [23]. However, chemical inhibitor interference with sand particles particularly in oil and gas wells depends on various parameters including inhibitor properties and the erosiveness and corrosivity of system [24].

CHAPTER 2

LITERATURE REVIEW

2.1 Review of literature on Slurry Erosion Corrosion

In recent years researchers have investigated the study of erosion corrosion phenomenon because of the serious problem of wear caused by EC which results in material loss, damage to the equipment and their failure in service. This type of problem usually occurs, where there is an interaction between target material, corrosive fluid and solid particles, especially in oil and gas transportation and processing plants, power generating plants, water treatment plants. Mostly this phenomenon could be observed for the valves, static equipments, piping systems, pressure vessels, heat exchangers, rotating equipments namely turbines, pumps, and compressors. There are different parameters that affect the erosion corrosion phenomenon, i.e. the fluid velocity, particle concentration, composition of the fluid that interact with each other and have significant effects on the materials performance in application. The complication and complexity of erosion corrosion does not only depend on interference of the different parameters, however a designer faced a range of problems when they are trying to attain required information on performance of a particular material. It is important to understand the erosion corrosion mechanism occurring in different metals (i.e. mild steel, carbon steel, stainless steels etc.) and how the fluid/particle, velocity, and impingement angle affects the erosion corrosion behavior of such metals.

2.2 Erosion Mechanisms

Finnie et al. 1960 [15], describes that it is unlikely to apply a single mechanism of material removal on all types of materials. G.P Tilly et al. 1969 [25], A. Levy et al. 1997 [2][16], discussed the ductile and brittle behavior of materials. In the case of ductile materials mass loss is done by micro-cutting and the plastic deformation or displacement by solid particles. Whereas, in brittle materials when particles hits the surface with a certain impact force, it produces cracks which propagate outwards from the impact point of solid particle. Hence there are two common categories for engineering materials that is ductile and brittle such as glass, aluminum and carbon steels etc. However so many other materials will not be easily classified based on their behavior.

2.2.1 Erosion by Ductile Behavior

Finnie et al. 1971 [26], make annotations on the erosion behavior of ductile metals, in which he presented a model for the erosion of ductile metals comprised on some assumptions. He suggested material removal in ductile metals should occur by a cutting process as in metal cutting or grinding. In this concept, a theoretical erosion particle strikes a target surface at a shallow angle, and its tip acts like the tip of a cutting tool, cutting away a swath of metal in front of it as it translates across the micro-surface. Fig 2.1 shows the predicted value of erosion from Finnie model. A.V Lavy et al. 1995 [27] shows that, the basic problem with this much-used micro-cutting model is that the erosion behavior of ductile metals, which the model was intended to depict, just does not occur in that physical manner, except for a few particles in a flow impacting at shallow angles i.e. 15°. So, A.V Lavy et al. presented platelet mechanism for the erosion of ductile metals.

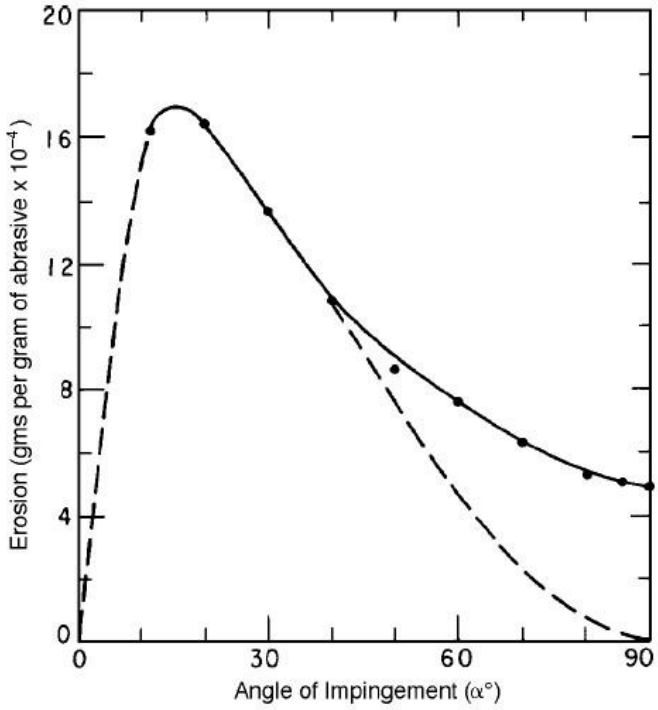

Figure 2. 1 Predicted value of erosion rate of pure aluminum (ductile metal) [25].

2.2.2 Platelet Mechanism of Ductile Metals

Alan Lavy et al. 1995 [27], describes the platelet mechanism of erosion for the ductile metals. The process is a straightforward one that involves common metal deformations including extrusion, pancake forging, bending, and fracture. SEM image Fig 2.2, shows that a number of flattened platelets over the hilly, center portion of the eroded area, with some bent and/or partially cracked areas. The hillocks are known to occur at steep impact angles. He presented the sequence of platelet formation and removal mechanism. Initially an eroded area with an extruded crater is formed followed by a single platelet that was extruded out of the crater on the right and flipped over the top of the crater, then a particle has struck the platelet and pancake forged it out, over part of the crater from which it was extruded. Particles have struck the platelet in a manner that has fractured its

attachment stem to the base metal, and it has been removed from the surface completely. He observed this sequence as the mechanism of erosion of ductile metals and has been observed countless numbers of times. Greg Hickey et al. 1985 [28], Thomas A. Adler et al. 1999 [29], and many other researchers after them reported that platelet mechanism Fig 2.3. Thomas Adler et al. studied the erosion behavior of the high chromium white cast iron eroded with tungsten carbide and small alumina particles. The erosion mechanism reveals that, it involves extrusion of thin platelets of white cast iron by the impact of the erodent particles. Furthermore the material is removed with the lip formation in the prior impacts followed by the flattening and fractured from the surface of the affected material by the subsequent impacts as discussed above by A. Lavy [26].

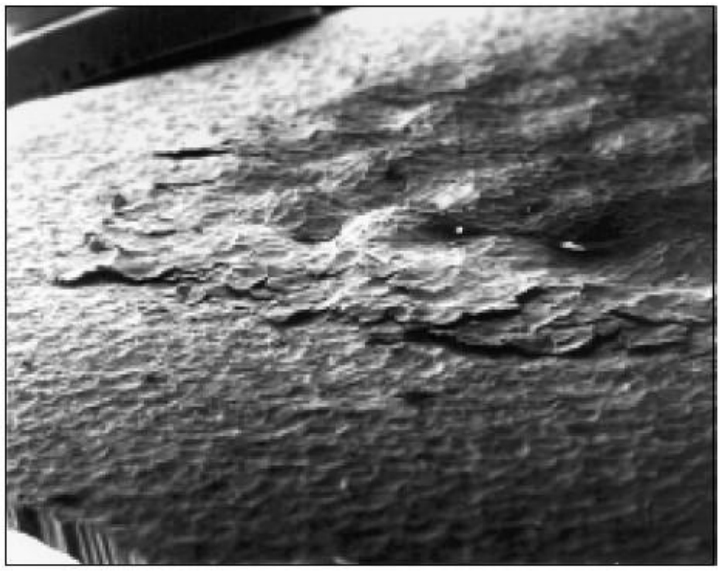

Figure 2.2 SEM image of aluminum eroded with steel shots [26].

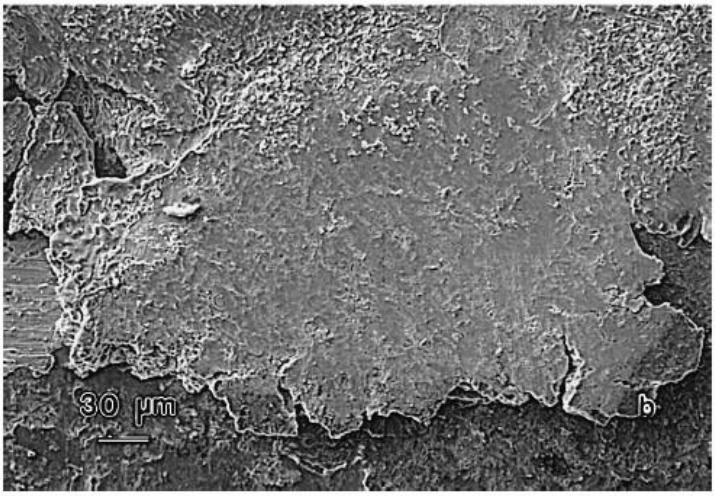

Figure 2.3 SEM image of hypoeutectic White cast Iron eroded by Tungsten Carbide [28].

2.2.3 Erosion by Brittle Behavior

It is observed by various researchers and accepted that erosion weight loss by solid particles in brittle materials is mainly from micro-cracking and fracturing of the surface material. Q. Chen et al. 2002 [30], shows the erosion weight loss as a function of impact angle Fig 2.4, and simulate the erosion of silicon carbide by the triangular particles. Particles were projected to the normal of the target surface. They observed the growth and propagation of cracks in horizontal and vertical directions. In case of sharp solid particles the cracks propagate much quicker in vertical direction as compared to the horizontal directions Fig 2.5 (a). However, horizontal cracking was increased if the eroding particle have larger angle because of the enhanced tensile stress component that is perpendicular to the direction of cracking. First radial cracks were formed and they propagate outwards from the outside edge of crack Fig 2.5 (b). A. G Evan et al. 1976 [31], studied the damage brittle solids and analyze them by fracture mechanics, he presented that first radial crack extension appears and then lateral cracks propagates through the Solids Fig 2.5 (c).

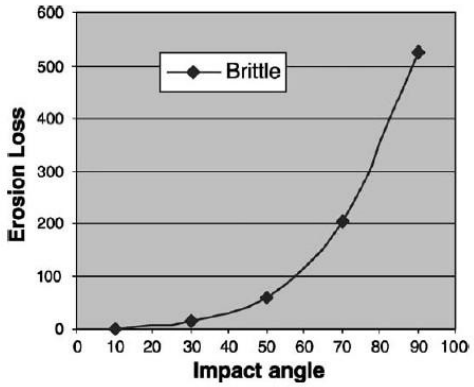

Figure 2. 2 Correlation between the impact angle as a function of erosion loss of brittle materials [29]

(a)

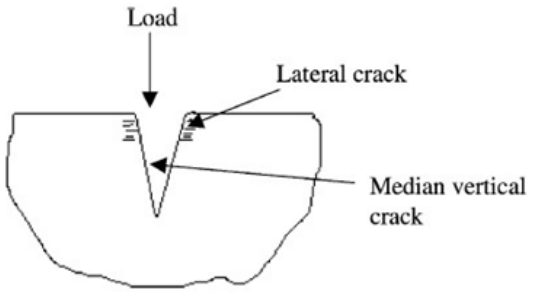

(b)

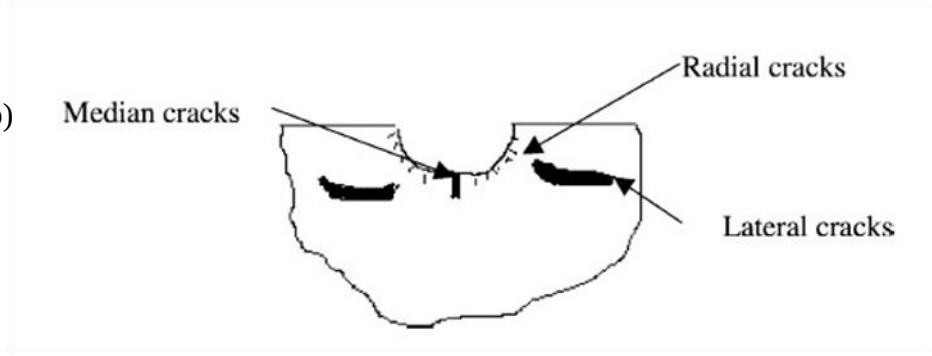

(c)

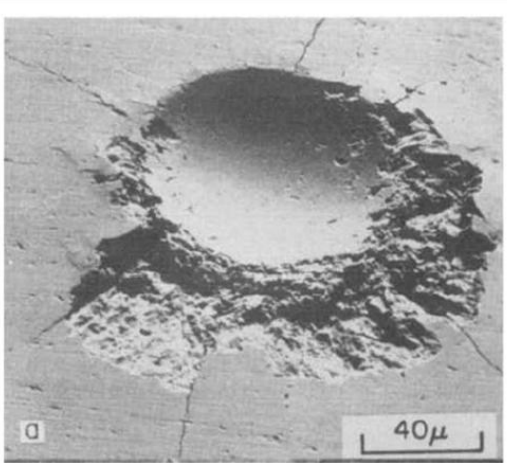

Figure 2.3 (a) Schematic representation of crack propagation by sharp tip particle, (b) crack propagation with a rounded particle, (c) radial cracks, [29].

2.3 Erosion Corrosion by Liquid-Solid Impingement

Material degradation causes by the impingement of fluid jet on the target surface, with or without solid particles is termed as erosion corrosion. The interactions of erosion and corrosion and their significance in aqueous systems has been reported by many researchers [2][8-12]. In general it is accepted that the summation of pure electrochemical and mechanical process is not greater than the effect, if electrochemical and mechanical erosion are acting in combination in certain environment. Such effect in combination is categorized as synergistic effect in which the conditions of liquid solid and liquid erosion shows the incremental weight loss, which cannot accounts for pure mechanical and electrochemical effects Fig 2.6.

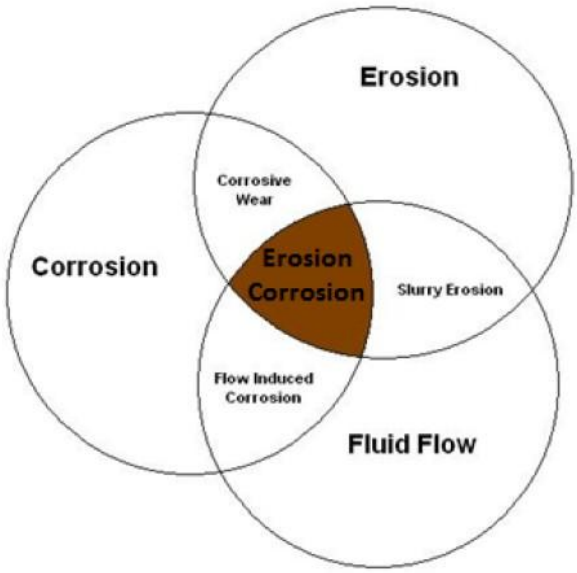

Figure 2.4 Schematic illustration of erosion-corrosion and fluid flow synergism [21].

2.3.1 Synergistic Effects of Erosion and Corrosion

A. Neville et al. 2005 [32], describes that because of synergistic effect, erosion corrosion in combination can remove the material in much greater amount than that damage if they consider them separately. The interactions are complicated and complex between these two processes, hence as such this becomes quite difficult to predict the life time of equipment and the material loss with much accuracy and reliability. Brent w. Madsen et al. 1988 [33] determine the synergism with slurry wear test apparatus for three type of materials in different conditions of test. He shows the data of synergism between the two components, the erosive wear component which he measured by cathodically protecting the surface and also the pure corrosion component from the total calculated wear which gives the amount of synergism. Furthermore he shows that as erosion enhances the corrosion rate, similarly corrosion process on the surface of specimen also promotes the erosive wear, which helps to deteriorate the metal quite easily.

2.3.2 Effect of Corrosion on Erosion

It is proposed by several researchers that the metal surface becomes rougher in result of corrosion; also erosive wear varies as a function of impingement angle of solid particles, so corrosion increases the roughness which actually promotes the rate of erosion with varying angle. Masanobu et al. 1990 [17] describes that corrosion accelerates the erosion rate by destroying the passive film layer and eradicate the work hardening layer by dissolution of the metallic surface which ultimately roughen the surface. In results of these effects the incoming particles when hit the surface, they could penetrate deeper in to the material, and hence corrosion actually promotes erosion wear damage.

Hutchings et al. 1995 [34], describes that in NaCl and acid slurries erosion is effected by corrosion through the disintegration of the flakes mainly by cracking induced by stress and corrosion. Material is plastically flowed because of the solid particles impact and it produces flakes. Sharp cracks propagate specifically at the roots of flakes and such cracks are developed by localized corrosion reactions, then as the incoming solid particles impinges on such surface, crack grows very quickly and flake detachment accelerates in result of that and ultimately it would leads to an enhanced erosion rate because of corrosion effects.

Baotong Lu et al. 2008 [35] studied the effect of ph on the surface properties in result of which corrosion enhanced erosion. They proposed that the corrosion-induced surface plasticity, which results from the interaction between electrochemical dissolution and the plastic deformation in surface layer. By experimental investigation they have indicated that the surface hardness degradation due to the corrosion-induced surface plasticity increases in direct relation with the anodic current density. The experimental result in their study shows that the surface hardness degradation depends not only on the anodic current density but also on the pH of corrosive media. In the acidic solution, the solution chemistry can also affect the surface hardness when corrosion occurs. This results in enhanced erosion rate.

2.3.3 Effect of Erosion on Corrosion.

Yugui Zheng et al. 1995 [36] studied the synergistic effect between erosion and corrosion in acidic slurry medium of five Steel. They found that as the velocity is increased there is a difference in electrochemical behavior, which is actually due to the effect of erosion on

corrosion and they demonstrate it in two distinct features: first the erosion (flow) increases the transport of the reactants on the surface of steel for example oxygen. Which may enhance the ability of passivation and re-passivation of SS or corrosion process could be increased in case of impassive steels (e.g. X60), and corrosion accelerates as the corrosion product leaves the metal surface. The second is that mechanical force is applied by the erosion process on the surface of steels, which breaks and weaken the passive film and strain difference cells would be formed on the surface which accelerates the corrosion rate.

J. Heidermeyer et al. 1981, [37] discussed the erosion effects on corrosion that is the mechanical effect of erosion or friction may stimulate chemical reactions between surface of solids and media surrounding it. He suggested that quite a lot of factors can promote this effect for example; plastic deformation produces the lattice defects, layers that are protecting the surface would be removed, heat of friction, increase in effective surface area, and faster transport of reacting particles. So because of these mechanical effects of erosion can activate the chemical or electrochemical reactions on the target surface.

G.T. Burstein et al. 2000 [38], observed sharp current rises during erosion corrosion process Fig 2.7. It is because of the breakage or removal of the oxide film on the surface by the erosive action of the abrasive solid particles and exposure of the bare metal surface to the solution for electrochemical reactions. They concluded that solid particle impingement stimulate the exposed metal surface corrosion reactions such as pitting in aggressive solutions.

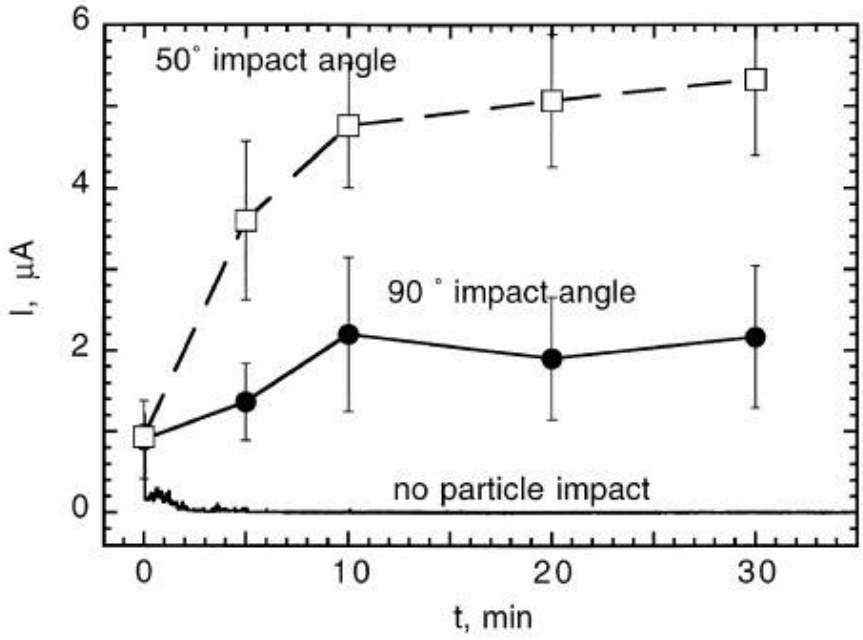

Figure 2.5 Variation of current with time during an impact of slurry with and without solid particles [37].

2.4 Erosion Corrosion Mechanism and Effect of Angle

It is well known after the investigation of many researchers, the erosion corrosion mechanism in ductile materials, play a major role by plastic flow whereas micro-fractures in case of brittle materials. However erosion corrosion behavior could be a combination of ductile and brittle materials and such behavior is expected in a two phase material containing a hard carbide phase with in soft ductile matrix.

G.T. Burstein et al. [38], studied the slurry erosion corrosion of 304L SS. They describes the three modes of material removal in slurry erosion corrosion, cutting mode I, that dominates in between 40° and 50°, Cutting mode II, which appeared below 40º, and indentation mode appears after 50°, these modes are also discussed by Neville, Shirazi. Also G.T Burstein (Fig 2.8) explained that the maximum erosion rate is in cutting mode I. With decreasing impact angle the erodent particle penetrates deeper in the surface and at the end of the scar a large lip could be created. The solid particle impinges on these extruded lips repeatedly and hence flakes developed on the eroded surface. This justification is inconsistent with the explanation that at glancing angles erosion produces rougher surface as compared to the incidence of normal angles. Furthermore at lower angles of impingement larger bare metal area is generated which results increase in erosion enhanced corrosion process. Hence in other words synergistic effects are more prominent at lower angles as compared to normal impacts.

In cutting mode II solid particle impacted and scratches the surface of metal along with cutting process is in action. In this mode erosion rate is decreased because in plastic deformation the loss of impact energy of the particles is very less. So the material is piled up at the end of the scar however the lip size is smaller as compared to that in cutting

mode I. Hence in cutting mode II, on the eroded surface, the flakes are less developed that resulted in the decrease in corrosion enhanced erosion. However in indentation mode passivation film remains intact on scar, it rarely breaks as the impingement angle tends towards 90°. So they observed minimum erosion corrosion effect at that 90° angle.

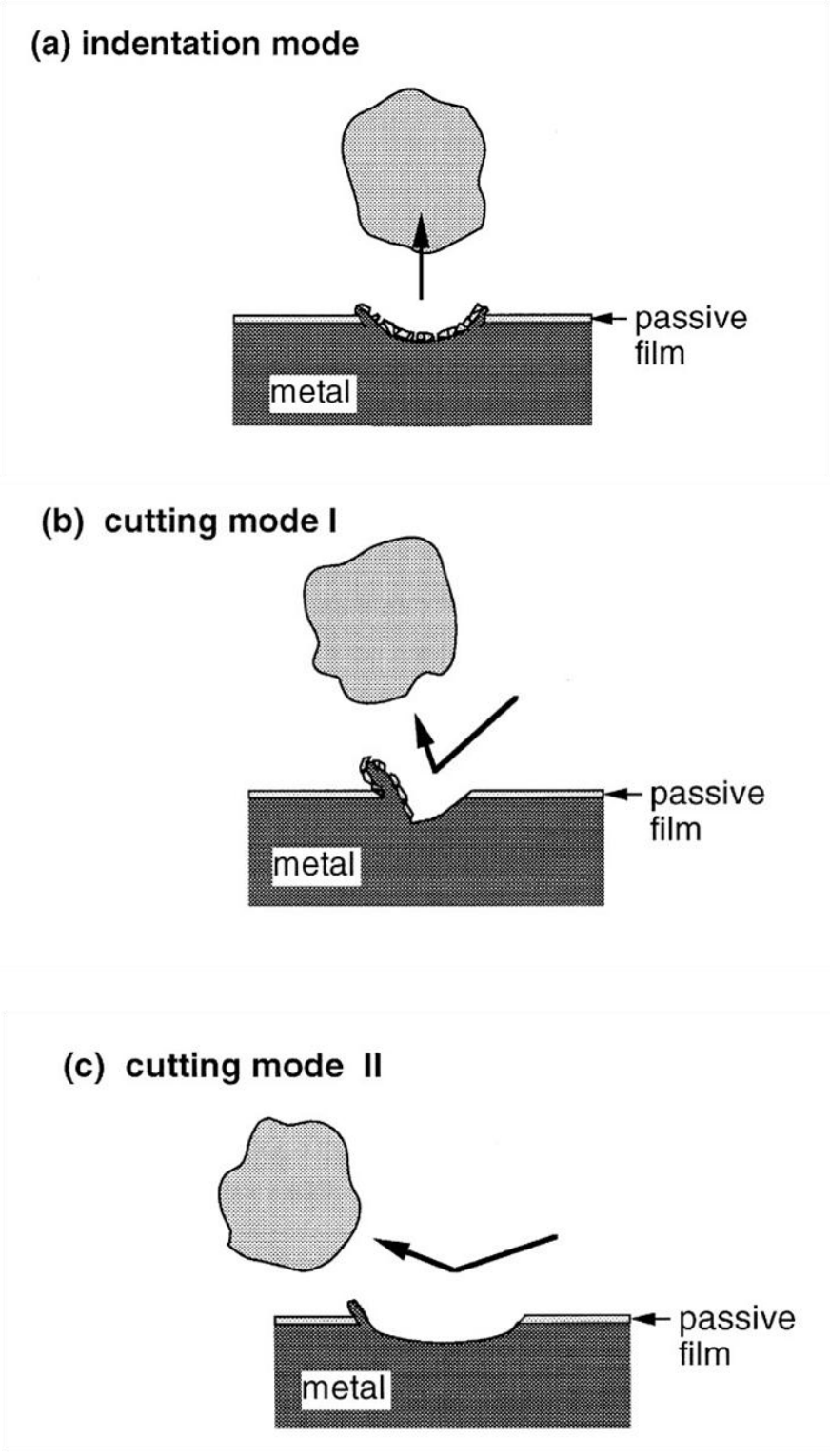

Figure 2.6 Schematic illustration shows three different types of plastic deformation by particle impact [37].

G.P Tilly et al. [25], shows this maximum erosion value comes at around 15° angle instead of 45°, this value differs because the carrier medium is gas instead of liquid. G.T. Burstein et al. [38] and Fuyan Lin et al. [19], explained that when stream of fluid impinges on the surface, it will spread out along the surface. This spreading effect is as shown in Fig 2.9. As the viscosity of fluid is very small (1.84 x 10 -4 $gs^{-1}cm^{-1}$), the solid particle directions in case of gas carrier fluid will not disturbed by spreading effect of the fluid flow. Whereas in the case of aqueous slurry as they have high viscosity value approximately (1.0 x 10-2 g $s^{-1}cm^{-1}$), the abrasive particle direction will be in the direction of fluid flow, and this effect is more prominent if the particle size is small. So in case of aqueous slurries fluid takes the original direction of flow and also the solid particles follow the same directions in slurries. The nominal impingement angle at which the slurry erosion rate reaches the maximum (Fig 2.10) is usually higher than the definite impingement angle of the solid particles. This explanation reveals that when the carrier fluid is liquid as compared to gas, the higher impact angle is required to produce the peak erosion rates.

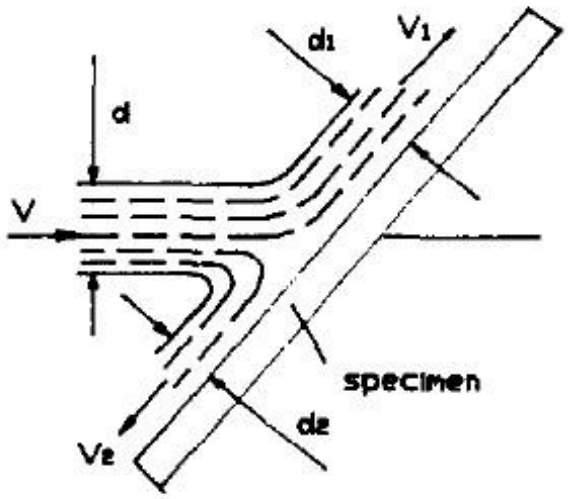

Figure 2.7 Schematic representation of a stream of flow impinges on the surface [38].

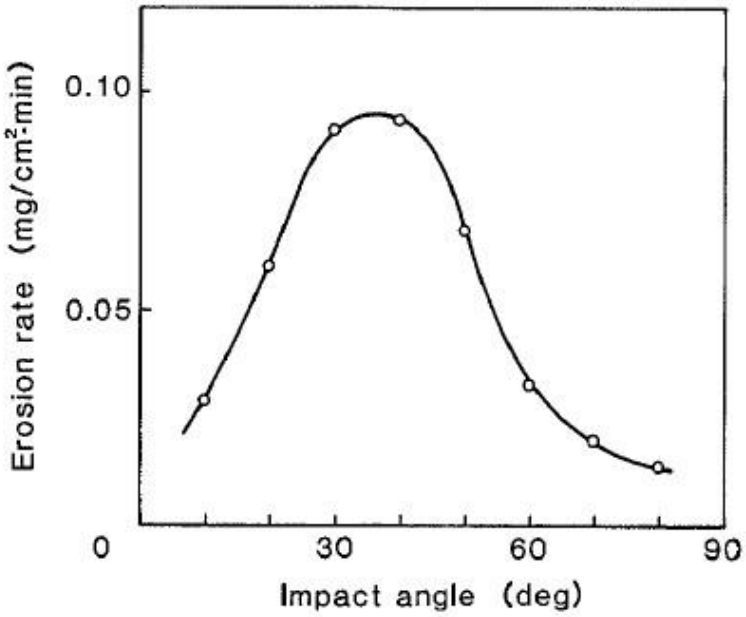

Figure 2.8 Effect of impact angle on erosion rate of 304 SS at 3 m/s velocity [16].

2.5 Effect of Fluid and Flow Velocity on Erosion-Corrosion

Neville et al. [32] revealed that as the fluid impinges on the flat surface, two regions on the surface could be observed, that the named stagnation region and wall jet region. They found that flow will not be disturbed by the presence of impingement surface and it will be mainly in the axial direction. They showed the erosion corrosion in wall jet area/region will be enhanced by the increment in the solid particle introduction in the slurry. Neville and C Wang et al. [39] Under the impinging fluid, showed the track of the particles and their trajectories at the surface they revealed that between stagnation region and wall jet region the sample is subjected to different kinds of damage such as chipping, cutting, ploughing and plastic deformation.

In another study S.A. Shirazi et al. [40], use CFD methodology for erosion prediction. They found that the W shape surface profile is produced due to the influence of fluid flow because of sand particles in slurry flows. It was found out that at the point on the surface of target, where fluid reaches first, at that point the velocity of the fluid reduces to zero. This is the central region of the eroded area, and hence named it a stagnation point. So in this region of stagnation, less mass loss was found because of the reduction in the speed of the particle impact. After that point or close to that point fluid flows radially and increases the speed of the particles on the target surface which results in the severe eroded regions and produces w shape of the scars. Whereas if the carrier medium of the solid particles is the gas, U shape of the wear scars produced because particles in this case can cross the fluid stream lines.

Hector et al. [41], studied the effect of flow field in slurry erosion, they explained that the fluid flow filed depends in first illustration on geometry of the target surface and the

regions in its surroundings. A particle that is suspended in an ideal and steady state liquid and as it approach the target that will be diverted from its original straight path because it experience the drag force as it moves along the surface. However particles that are more dense and have higher velocity in low viscosity fluids will be less affected after the direct collision from the specimen, furthermore particle that are less dense and are moving with slow velocities will be mostly follow the streamlines of the liquid and avoid collision with the surface in the stream of fluid (Fig 2.11). They also mention some of the factors that affect the slurry erosion because of the flow field, target-particle velocity, and angle of impact, boundary layer properties, particle-particle, interactions, particle rebound, Reynolds number, size and shape of target.

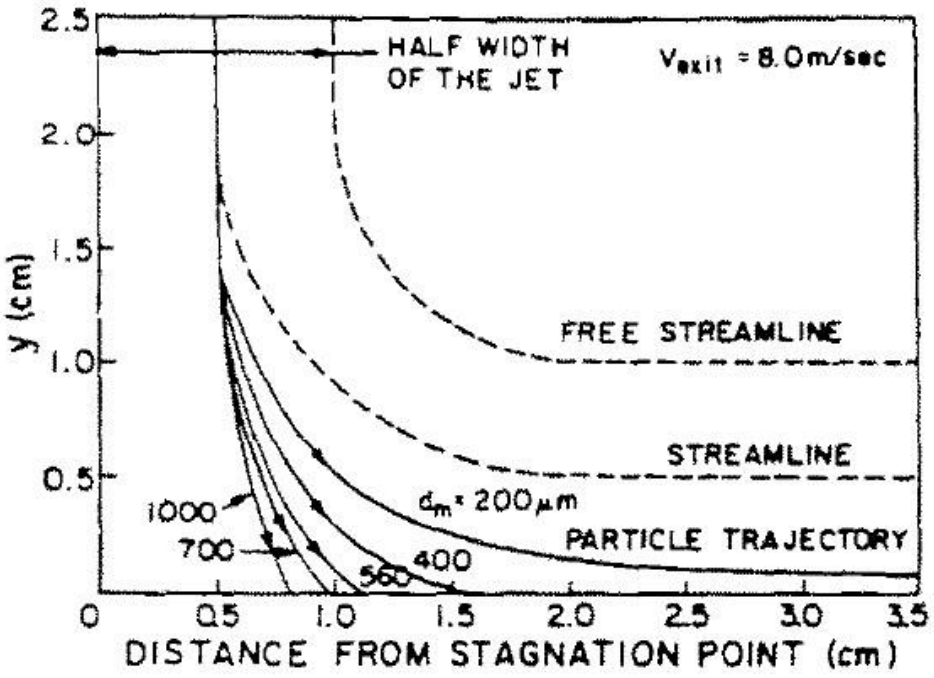

Figure 2.9 Sand particles trajectories of different diameter in a jet of water directed at flat plate.

2.6 Discrepancies in Erosion Corrosion Rates

Comparison of erosion corrosion resistance of two ductile materials having difference in their ductility has been rarely investigated under a range of conditions i.e. variety of impingement angles along with a fluid velocity. G. Sundararajan et al. [42] studied the differential effect of the hardness of metallic materials (1045 steel and tool steel) on their erosion resistance and shows that irrespective of the composition of the steel, the impact velocity, impingement angle and the nature of the erodent particles, the erosion resistance of the steels remains constant or even slightly decreased with increasing hardness. Sundararajan explained that in erosion particles have very short time of contact. Hence the deformation is in fully adiabatic condition. Under adiabatic conditions any increase in strength results in the decrease in the critical strain for localization. he also suggest that maximum erosion rate as a function of impingement angle depends on the coefficient of friction i.e. with increasing the coefficient of friction peak erosion rate shifted towards lower impact angles. Similarly Sergio Crnkovic et al. [43], carried out sand water slurry erosion of quenched API 5L X65 steel, he showed that there is a slight tendency that larger hardness leads to smaller erosion rate, and peak erosion rate comes out at 30° then it decreases to 90º. Hutchings et al. [44] studies the erosion rate for three ductile metals copper, aluminum, and mild steel he suggest that erosion rate decreases as the hardness increases and reaches to peak erosion rate around 30° to 40°. Also C. Allen et al. [45] concluded that hard metals exhibit decreasing erosion rates with an increase in hardness and peak erosion rate shows at 60° to 75°. Furthermore A. V. Levy and G. Hickey et al. [46] studied the liquid solid particle slurry erosion of A53, 304 Steels and discussed that as the ductility of the alloys tested in gas solid erosion increases, erosion

rate decreases however no such correlation possible in liquid solid particle erosion behavior. Also Fuyan Shao et al. [19] demonstrates the peak erosion rate depends on air or liquid based on their viscosity, he concluded that higher the ductility the smaller the peak erosion angle. This is also shown in by J Malik et al. [47] in his study that 1020 carbon steel peaks at 30° in case of air.

Contrary to above finding A. V levy et al. [48] reported that, greater the ductility generally results in lower erosion rates. This is because of the ability of ductile material to absorb impact energy at higher angle. Furthermore, M.M stack et al. [49] suggested that, as harder material have inability to maintain an adherent and protective oxide scale. The erosion corrosion resistance is decreased in harder material. In recent study by J. Neshati et al. [50] on X65 steel, he showed that maximum erosion corrosion comes out at 25°. Where as in another study conducted by G.T Burstain et al. [38] for pure iron and 304 SS gives peak erosion corrosion at 30° to 50° where as for aluminum by tab water slurry peaks between 40° to 50°. Based on the above studies, there are some contradictions between the erosion corrosion characteristics of different ductile materials. Hence the objective of this study is to compare the ductility effect on erosion corrosion rate of two pipeline steel grades under varying operating conditions of impingement angles, jet velocity and solid particles introduction. The study aims to quantify the effect of erosion on corrosion and to understand the mechanism involved in erosion enhanced corrosion behavior. In addition, the study provides a data base to predict some correlations based on such realistic predictions of erosion corrosion behavior in various conditions.

2.7 Erosion Corrosion Models

Sand is commonly produced along with production fluids (oil and gas), and this is a major problem for the oil and gas industry. Sand production is a concern, since it can bring about a variety of problems. There are three main problems i.e. pressure drop, pipe blockage, and erosion. Sand erosion can cause failure of equipment, leaks in pipelines resulting in environmental disasters and potential injury to personnel. Therefore, predicting solid particle erosion rate is a helpful tool in designing and selecting equipment to prevent failures. Predicting solid particle erosion in gases and liquids is a challenging task, however we don't have a model that can be utilized for erosion corrosion rate prediction for all conditions and materials. Hence this section will review some of the popular models, a variety of models and approaches have been proposed by researchers, Finnie et al. [26], Hutchings et al. [51], Sundararajan et al. [52], Bitter et al. [53], and many others. Usually, erosion prediction models are divided into three categories: empirical, mechanistic and CFD based. Since erosion is complicated, most proposed erosion prediction models are a combination of all these categories.

2.7.1 Erosion Models for Ductile Metals

Since the pioneering work of Finnie et al. 1960 [15], there have been various attempts worldwide to derive a correlation between the erosion rate and the parameters used, in a mathematical form. In the literature, modeling erosion of ductile metals was treated separately for the oblique impact and normal impact of erodent particles, because of the mechanism involved in the two processes are entirely different. It is unanimously agreed that oblique impact erosion occurs by a cutting mechanism and Finnie's models [26],

have been developed for oblique impact erosion. For normal impact erosion, although the particle impacts cause plastic deformation of the substrate, various schools of thought exist in identifying the exact manner of materials removal.

2.7.2 Oblique Impact Erosion Model

At lower impingement angles, Finnie et al. [26], explains the removal of material that is swept by tip of solid particle as a result of plastic deformation. When the horizontal movement of the solid particle stops or if the tip of angular particle leaves the surface, the micro cutting action will be ceases.

$$E = \left(\frac{f_c}{2k}\right)\frac{D_t U_i^{\,2}}{0.9272 H_s}\left[Sin2a - \frac{8}{k}Sin^2 a\right] \quad \tan a \le k/8$$

$$E = \left(\frac{f_c}{16}\right)\frac{D_t U_i^{\,2}}{0.9272 H_s}\left(Cos^2 a\right) \qquad \tan a \ge k/8$$

Where, f_c is the percentage of particles impinges the surface cutting in an idealized way. U_i is the solid particle impingement velocity, D_t and H_s are the density and static hardness of target material respectively, and α is the particle impingement angle. K is the ratio of vertical to horizontal force components on the particle, and was assumed as a constant

2.7.3 Normal Impact Erosion Model by Hutching.

At normal impact, the erosion for ductile material at normal impact by spherical particle occurs by the formation and subsequent detachment of platelets of metal lying parallel to the eroded surface. Hence, the model developed by Hutchings et al. [51] suggests that

detachment of platelets is only possible when the accumulated plastic strain within the fragment, after many cycles of plastic deformation, reaches a critical value, and the final expression for dimensionless erosion rate has been shown below.

$$E = 0.033 \frac{\alpha_f D_t D_p^{1/2} U_i^3}{\varepsilon_c^2 H_d^{3/2}}$$

Where, H_d and D_t is the dynamic hardness and density of the target material respectively, D_p is the density of erodent particles, and U_i is the erodent particle velocity. The term α_r/ε_c^2 cannot be measured independently. Hutchings assumed the value of α/ε_c^2 is equal to 0.7.

2.7.4 Normal Impact Erosion Model by Sundararajan.

Sundararajan and Shewmon et al. [52] derived an equation for normal impact, on the basis of significant strain criteria for the erosion to take place. They consider the fact that after the certain amount of solid particle impinges on the target surface, the material will be removed by the removal of localized extruded lips along the craters, which are formed after various impacts. The lips that are formed after certain number multiple impacts were assumed to be removed on the basis of critical strain and that strain is attained after a number of particle impacts. They consider the thermo-physical properties of material that is under considerations for erosion; hence the final expression for dimensionless erosion can be given as:

$$E = \frac{6.5X10^{-3}U_i^{2.5}D_p^{0.25}}{C_p T_m^{0.75} H_s^{0.25}}$$

Where U_i is the velocity of impacting particles. D_p, C_p, T_m, H_s are the density, specific heat, melting temperature, and static hardness of the target material.

CHAPTER 3

MOTIVATION AND OBJECTIVES

3.1 Motivation

Erosion corrosion is a serious problem in offshore to health care industries. Billions of dollars are spent annually due to damage caused by erosion corrosion. This problem could enhance the serious concerns to processing and operations along with project economic issues, especially where precise corrosion rate prediction is required. Literature review indicates that though so many resources have been used to investigate erosion-corrosion; however the mechanism of erosion corrosion is still not fully understood. So therefore, detailed parametric study can help predict erosion-corrosion which can cut down the damages, losses and serious threats to the safety of operators.

AISI 1030 and API 5L-X65 carbons Steels are commonly used in oil and gas production, refining, marine applications, petrochemicals, polymer production, synthesis, chemical processing, desalination plants, and transmission pipelines. However for such materials erosion corrosion phenomenon have a serious concern for their life. Hence these steels have been selected for in-depth erosion corrosion investigation with and without solid particles. Furthermore we need to have an in-house impingement erosion corrosion database, which can be later used to develop a prediction tool for different industrial applications.

3.2 Objectives

Objectives are defined as follows:

1. To develop impingement erosion corrosion database for AISI 1030 and API 5L-X65 carbon Steels.

2. To quantify the effect of fluid jet velocity, various impingement angles and solid particle introduction.

3. Understanding the mechanism of impingement erosion corrosion based on different characterization tools such as FE-SEM and optical profilometer.

4. Development of impingement erosion corrosion correlations based on above experiments.

CHAPTER 4

MATERIALS AND RESEARCH METHODOLOGY

4.1 Impingement Erosion Corrosion Apparatus.

The Impingement corrosion and erosion-corrosion testing of AISI 1030 & API 5L X65 steel specimens were carried out using a Flowloop test rig. It has a wide range of testing capabilities. To evaluate the Impingement corrosion and erosion-corrosion resistance of materials under high-speed flow and to investigate the damage mechanism of steels involved. So therefore, a multipurpose-flow loop was manufactured locally to carry out the detailed investigation.

Fig 4.1 shows the actual picture of the apparatus. The nozzle diameter is 3 mm and it is circular in shape, its material is 316L Stainless steel, as shown in Fig 4.2 (a). All of the metallic material piping system, solution tank, cyclone separator, valves, pump blades are made up of stainless steel 316L. Fluid jet velocity was calculated using ultrasonic water flow meter, Model: Wprime-280W, Fig 4.2 (b). The pressure gauge Fig 4.2 (c), which was used for velocity calculation, using energy equation. Pump speed was controlled by a 650V variable frequency drive control panel that is shown in Fig 4.3 (d.) Taylor 9940N temperature gauge was used to monitor the temperature Fig 4.2 (e). A stainless steel 15Kw pump (Lowara Company) was used for pumping of the fluid Fig 4.2 (f).

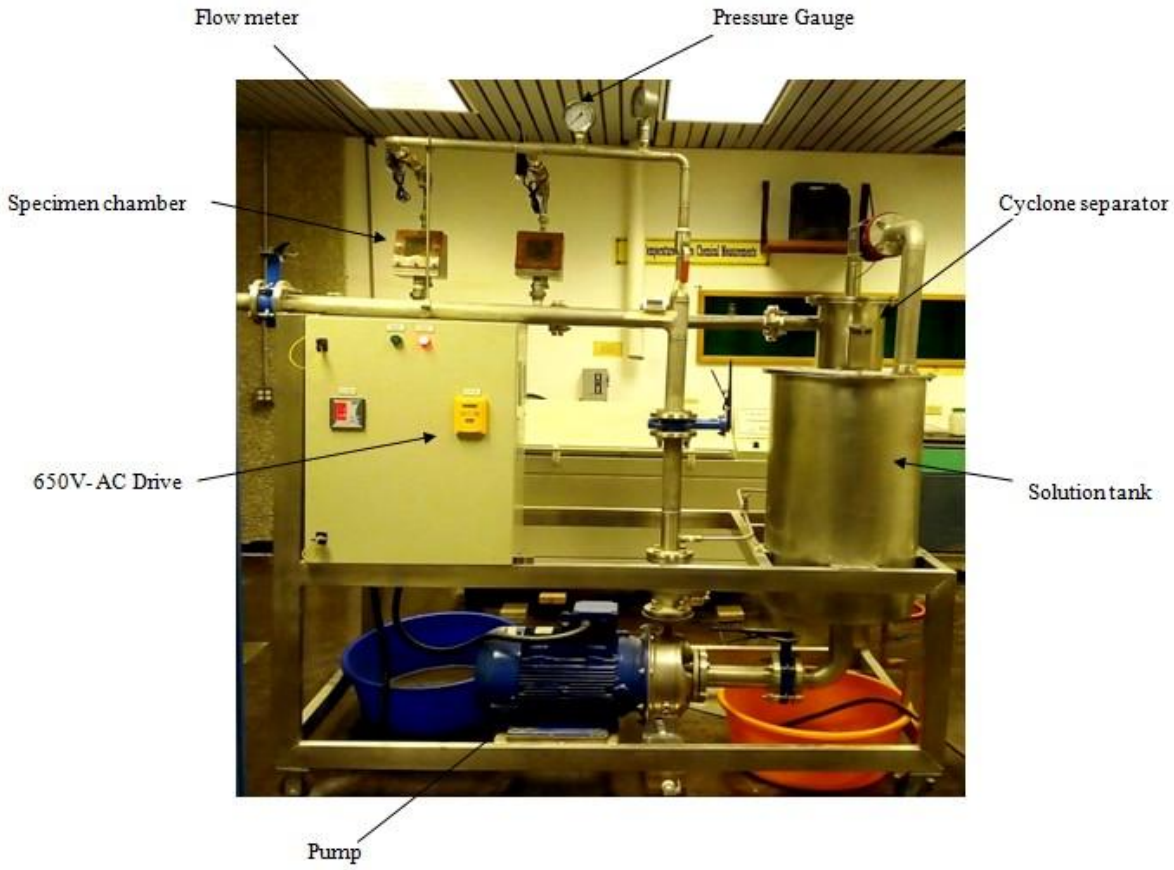

Figure 4.1Multipurpose Flow loop manufactured locally.

a. Nozzle

b. Flow meter

c. Pressure gauge

d. VFD drive 650V
Control panel

f. Pump

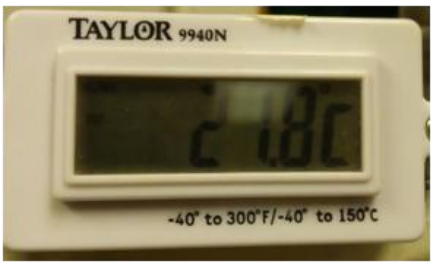

e. Temperature gauge

Figure 4.2 (a-f) Different instruments installed on flow loop.

4.1.1 Fluid Jet Velocity Calculation

Velocity of fluid jet, impinging on the surface was calculated by using the energy equation as explained below. Energy equation has following relation:

$$\frac{P_1}{\gamma} + \frac{V_1^2}{2g} + Z_1 = \frac{P_2}{\gamma} + \frac{V_2^2}{2g} + Z_2 + \sum h_L \quad \text{..... eq (1)}$$

We can put V1 in terms of V2 by using relation:

$$A_1 V_1 = A_2 V_2$$

$$\Rightarrow V_1 = \frac{D_2^2}{D_1^2} V_2 \qquad \text{Or} \qquad V_1^2 = \frac{D_2^4}{D_1^4} V_2^2$$

Since D1 is the diameter of pipe where as D2 is the diameter of the nozzle. So by putting value of V1 in terms of V2 in equation (1), we have following relation:

$$\frac{P_1}{\gamma} + \frac{D_2^4 V_2^2}{D_1^4 2g} + Z_1 = \frac{P_2}{\gamma} + \frac{V_2^2}{2g} + Z_2 + \sum h_L$$

We assume that at nozzle point pressure P2 is approximately zero (atm.) and also (Z1-Z2) can be negligible and flow is assumed to be laminar.

Now we know that:

$$h_L = \frac{fLV_1^2}{D_1 2g} \qquad \text{And} \qquad f = \frac{64}{\text{Re}} \qquad \Rightarrow f = \frac{64}{\frac{\rho V_1 D_1}{\mu}} \qquad \because \text{Re} = \frac{\rho V_1 D_1}{\mu}$$

$$\Rightarrow h_L = \frac{32\mu L V_1}{\rho g D_1^{\,2}} \qquad \text{Hence,} \qquad h_L = C_2 V_1$$

So, first equation of energy becomes:

$$\frac{P_1}{\gamma} + \frac{D_2^4}{2D_1^{\,4} g} V_2^2 = \frac{V_2^2}{2g} + C_2 V_1$$

$$\Rightarrow \frac{P_1}{\gamma} = \frac{V_2^2}{2g} - \frac{D_2^4 V_2^2}{D_1^4 2g} + C_2 V_2 \frac{A_2}{A_1} \qquad \because \mathrm{V}_1 = \frac{A_2}{A_1} V_2$$

$$\Rightarrow \frac{P_1}{\gamma} = V_2^{\,2}\left(\frac{1}{2g} + \frac{D_{ratio}}{2g}\right) + C_2 V_2 \left(\frac{D_2}{D_1}\right)^2$$

$$\Rightarrow \frac{P_1}{\gamma} = V_2\left[V_2\left(\frac{1}{2g} + \frac{D_{ratio}}{2g}\right) + C_2\left(\frac{D_2}{D_1}\right)^2\right] \quad \text{..... eq (2)}$$

Now for the above equation we have, P1 equal to 1 bar. Also we have the values of D ratio and C2 values. So only unknown is V2, which is velocity at nozzle point.

Calculation of C2 value and Dratio is as follows:

$$\rho = \text{Density of water} = 1000\,\text{kg/m}^3$$

$$D_1 = \text{Diameter of Pipe} = 1\,\text{inch (ID)} = 0.0254\,\text{m}$$

$D_2 = \text{Diameter of Nozzle} = 3\text{mm} = 3 \text{ x} 10^{-3} \text{ m}$

$P_1 = \text{Pressure at point } 1 = 1 \text{ bar} = 10^5 \text{ pa or } 10^5 \text{ N/m}^2$

$\gamma = \text{Specific gravity} = 9810 \text{ N/m3} \quad \{1\text{N} = 1\text{kg m/s}^2\}$

$\mu = \text{Dynamic Viscosity of water} = 8.90 \text{ x} 10^{-4} \text{ pa.s} \quad \{\because 1\text{pa} = 1\text{N/m}^2\}$

$L = \text{Length of pipe from point } 1 \text{ to } 2 = 4.5 \text{ ft} = 1.371\text{m}$

$g = 9.8 \text{ m/s}^2$

$$D_{ratio} = \left(\frac{D_2}{D_1}\right)^4 = \left(\frac{3 \text{ x} 10^{-3} m}{0.0254 m}\right)^4 = 1.9460 \text{ x} 10^{-4}$$

$$C_2 = \frac{32 \mu L}{\rho g D_1^2} = \frac{32 \text{ x } 8.90 \text{ x } 10^{-4} \text{ pa.s x } 1.371\text{m}}{1000 \text{ kg/m}^3 \text{ x } 9.8 \text{ m/s}^2 \text{ x } (0.0254\text{m})^2}$$

$$\Rightarrow C_2 = 6.2974 \text{ x} 10^{-4} \text{ s}$$

Now by putting values in equation 2 we have:

$$\frac{10^5 \text{ pa}}{9810 \text{ N/m}^3} = V_2\left[V_2(0.0511)s^2/m + 8.784 \text{ x } 10^{-6}\text{s}\right]$$

$$10^5 m = V_2{}^2(502.22)s^2/m + 0.08617V_2 .(\text{s}) \quad \{\because 1\text{pa} = 1\text{N/m}^2\}$$

$$\Rightarrow 502.22V_2{}^2 + 0.08617V_2 - 10^5 = 0$$

$$\Rightarrow V_2 = \frac{-0.08617 \pm \sqrt{(0.0861)^2 - 4(502.22)(-10^5)}}{2(502.22)}$$

$$\Rightarrow V_2 = \frac{14173.41}{1004.44}$$

Hence $V_2 = 14.110$ m/s

We can calculate the required value of pressure by putting the known values in equation 2, that should be set on pressure gauge by varying the pump speed to get our under consideration jet velocity.

4.2 Test Samples and Sand Particles Characterization

4.2.1 Test Samples

Erosion corrosion testing was performed on AISI 1030 and API 5L X 65 carbon steels. The elemental composition was evaluated using spectromax metal analyzer Fig 4.3 (a). and detailed composition is presented in table 4.1. These two grades selected because of their immense use in petroleum, desalination and many other industrial pipelines. The carbon steels in general have very good physical properties such as: ductility, enormous strength, weld-ability, and amenability to heat treatment to achieve various mechanical properties. The Vickers hardness (HV) at room temperature using a CSM Micro Combi Hardness tester (Diamond Indenter) was used to measure under 2N loads (P) over an indentation time of 10s. Average hardness value of AISI 1030 was 304 HV and for X65 it was 298 HV. All samples were machined to 20 x 20 x 5 mm size. Followed by hot mounting in Lucite material, to make sure that only unit area (20 x 20 mm) is expose to fluid jet and grinded up to 600 grit size paper to get surface average roughness of less than one micron Fig 4.3 (b). Before every experiment, the samples were cleaned with acetone, dried with master heat gun drier, and weighed to an accuracy of 0.01 mg using Starter weighing balance.

(a)

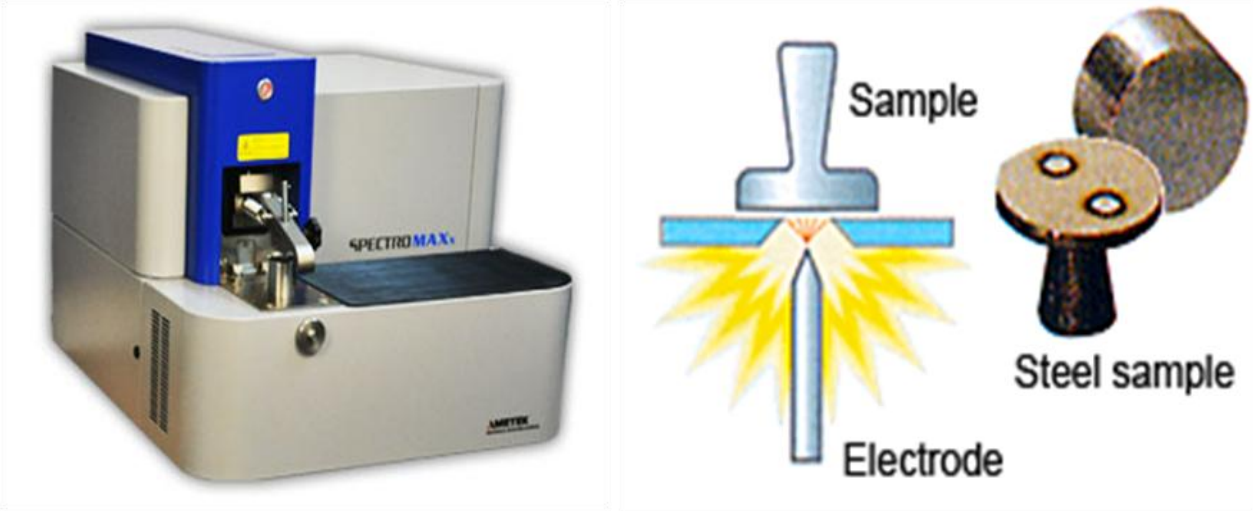

(b)

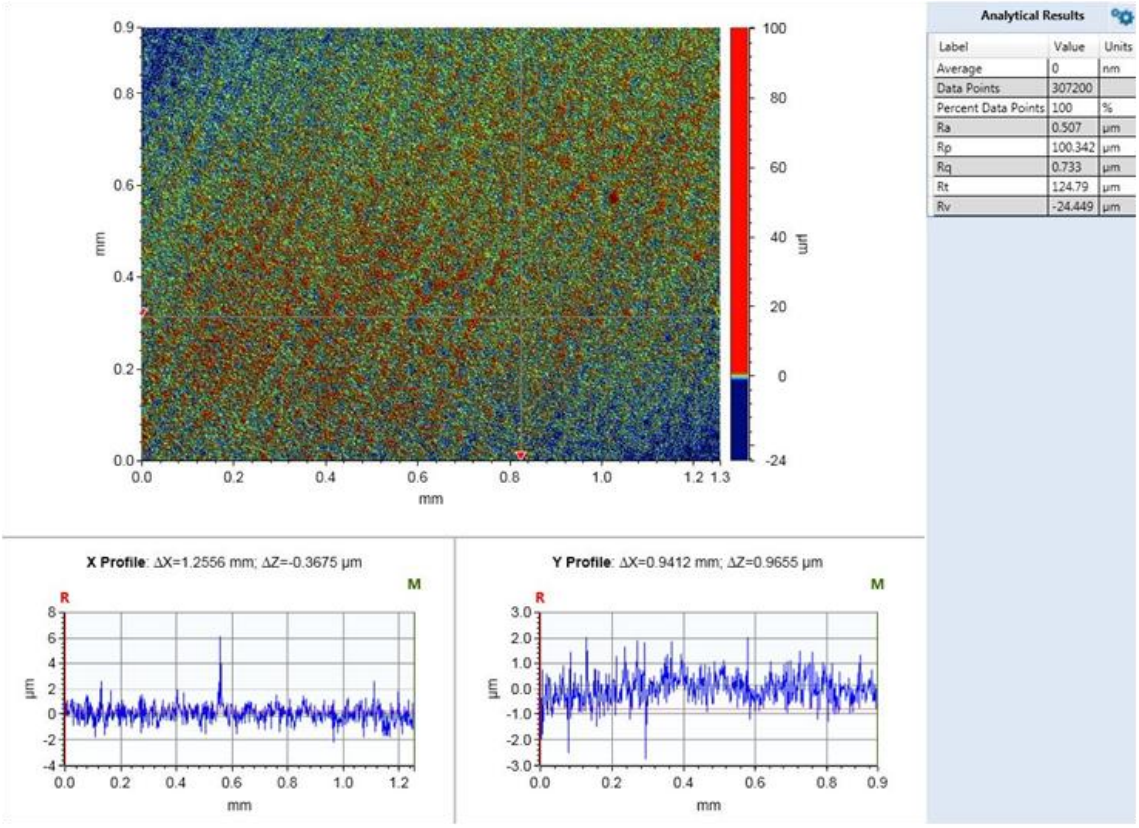

Figure 4.3 (a) Spectromax metal Analyser (b) surface roughness (Ra: 0.5 micron) and its profile.

Table 4.1 Composition of AISI 1030 and API 5L-X65 Steels

Elements		C	Mn	Fe	Cu	Mo	Ni	Cr	V	Co	P
% Compositions	AISI 1030	0.29	0.651	98.2	0.147	0.0377	0.086	0.0709	0.108	0.01	0.0015
	API 5L X65	0.165	1.29	98.1	0.0548	0.0092	0.0183	0.0275	0.0076	0.0063	0.0015

4.2.2 Sand Particles

Figure 4.4 (a-b) shows SEM images of pure silica sand particles utilized in impingement erosion-corrosion experiments. Sand particle have a range of sizes from 125 microns to 704 microns, average particle size is 314 microns. These silica sand particles were taken from Riyadh region in Saudi Arabia, provided by BMS Company in Jeddah. Hardness of the silica sand was 1161 HV which is equivalent to Moh's hardness no of 7 on a scale of 10 [54]. Particle size distribution was analyzed by using particle size analyzer (Micro-Trac S3500). Mean size was 314 µm, and detailed statistical data for the size distribution of silica sand is shown in table 4.2.

Table 4.2 Statistical data of silica sand particle size distribution.

Particle size (µm)	125	148	176	209	248	296	352	418	497	592	704
Percentage	1.19	1.64	2.67	5.22	10.69	18.69	23.27	18.95	9.94	2.88	1.31

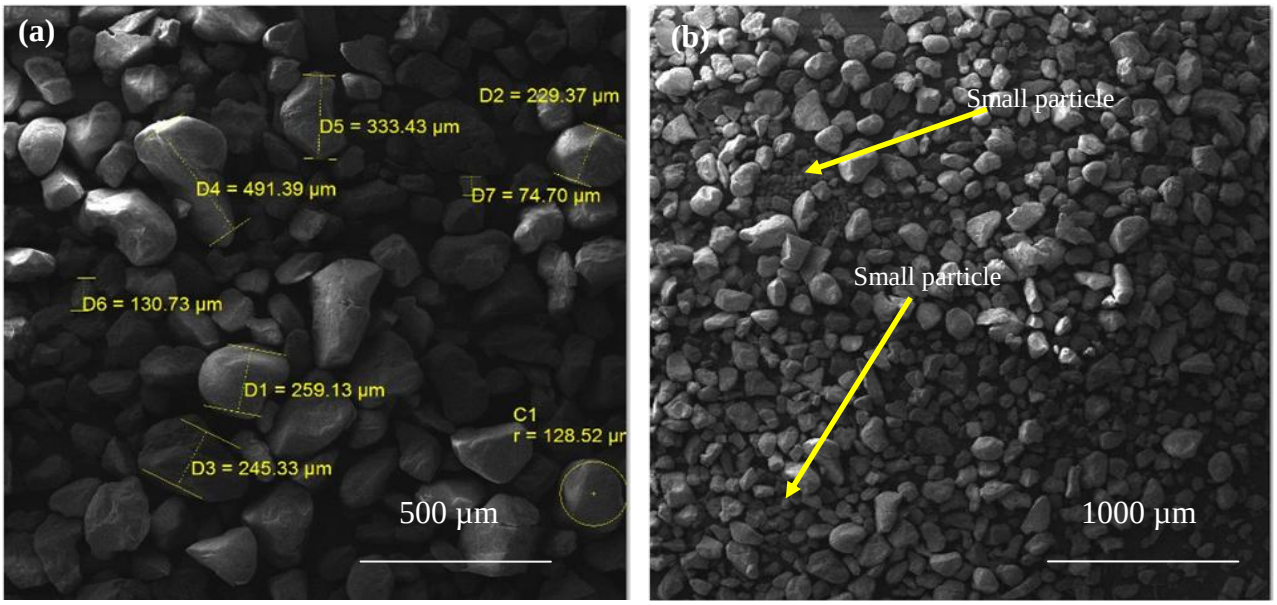

Figure 4.4 Silica sand abrasive particles (Average size 314 microns).

4.3 Test Procedure

Impingement erosion corrosion tests were performed according to ASTM-G-73-98 test standard [55].

1) Tap water from sweet water line was used in the experimentaion for the impingement of fluid jet. TDS and chloride content was determined by ultrameter. Total desolved salt and chloride content are given in table 4.3.

2) We calcuate the salt content which is required for approximately 69 liters of water to prepare 0.2 Molar NaCl solution. Solution preparation calculations are given in Fig 4.5. Impingemnt erosion-corrosion experimental plan with and without solid particles is shown in Table 4.4 a & b respectively.

3) Tested specimen were hot mounted, then cut into required dimensions, and ground on SiC paper upto 600 grit size (Fig 4.6).

4) After preparation and weighing of samples, they were fixed in specimen holders at certain angle (Fig 4.7) and put in test chamber under the 3mm diameter circular nozzle. Tests were carried out at three different velocities: 3m/s, 6m/s, and 12m/s. Velocities were calculated by using energy equation, and fluid pressure of the fluid upstream of the nozzle. under each velocity, behavior of the both types of specimens at five different impingement angles were examined: 15°, 30°, 45°, 60° and 90° respectively.

5) Weightloss method was utilized for the calculation of impingement erosion corrosion wear rate. The duration of each experiment was 24 hrs.

6) After experiment samples were cleaned by using soft tooth brush to remove corrosion product from its surface. Cleaned with acetone and dried with master heat gun to ensure the removal of moisture content. The weight loss after erosion–corrosion tests were

measured using a digital balance, accurate to 0.01 mg and corrosion rate calculation were done according to ASTM G1-03 [56] (Table 4.5). Each test was repeated at least two times. Steps of one test cycle is shown in Fig 4.8.

Table 4.3 Tab water analysis

Tap Water (Sweet)	
TDS	164.2 ppm
Ph	7.5
Chloride	140 ppm

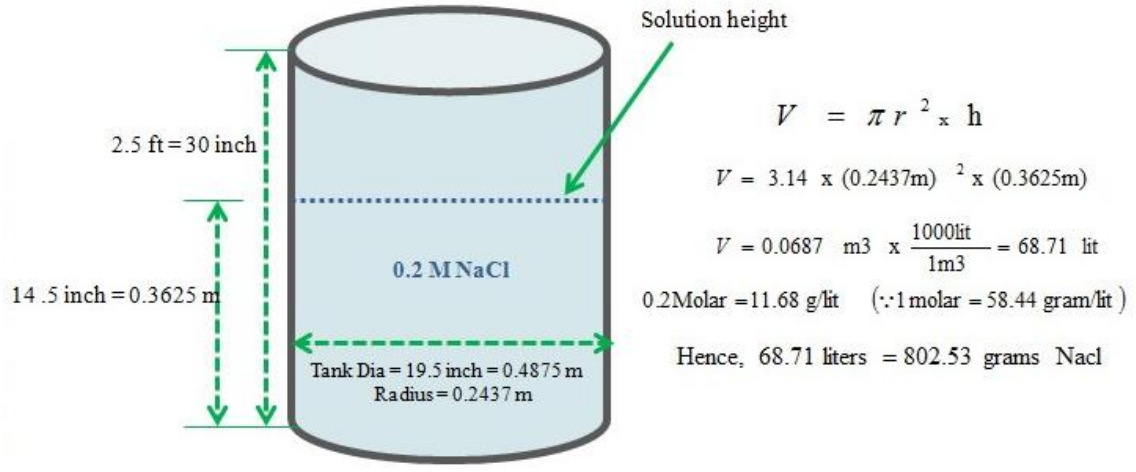

Figure 4.5 Solution preparation schematic and salt content calculation.

Table 4.4 (a) Impingement Corrosion, (b) Impingement Erosion Corrosion Experimental plan

(a)

Experimental Conditions (Impingement Corrosion)						
Solution		Tap water (0.2 M-NaCl)				
Nozzle distance to sample		5cm (50mm)				
Temperature		25 °C (Ambient)				
sample size		20 x 20 x 5 mm				
Sample Area		400 mm^2				
Velocity (m/s)		3,6, & 12m/s				
Impact Angle		15°	30°	45°	60°	90°
Mild steel	AISI 1030	2	2	2	2	2
Mild steel	API5L-X65	2	2	2	2	2
Samples Tested		60				

(b)

Experimental Conditions (Impingement Erosion Corrosion)						
Solution		Tap water (0.2 M-NaCl) 500ppm Silica sand (250 µm Av. Size)				
Nozzle distance to sample		5cm (50mm)				
Temperature		25 °C (Ambient)				
sample size		20 x 20 x 5 mm				
Sample Area		400 mm^2				
Velocity (m/s)		3,6, & 12m/s				
Impact Angle		15°	30°	45°	60°	90°
Mild steel	AISI 1030	2	2	2	2	2
Mild steel	API5L-X65	2	2	2	2	2
Samples Tested		60				

Figure 4.6 Sample after hot mounting and edge preparation.

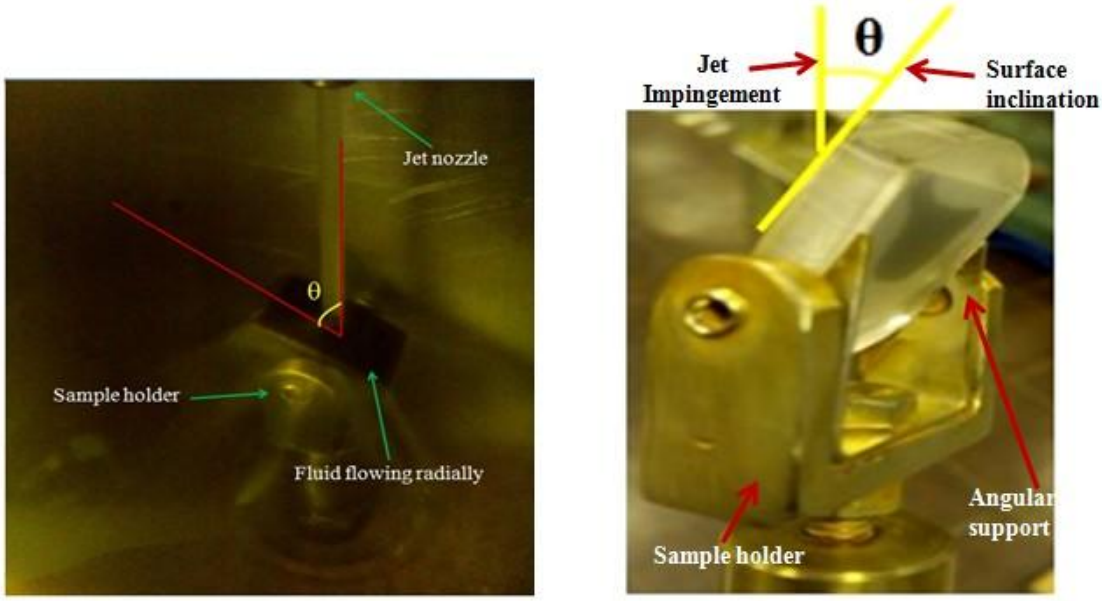

Figure 4.7 Sample fixation at a certain angle on angular support and under jet in test chamber.

$$\text{Corrosion Rate} = \frac{\text{Weight loss (mg/g)} * K}{\text{Density of sample (g/cm}^3) * \text{Exposed Area (cm}^2) * \text{Exposure time (hr)}} \qquad (eq.1)$$

Table 4. 5 corrosion rate calculation according to ASTM-G1-03

Desired Corrosion Rate Unit (CR)	Area Unit (A)	K-Factor
mils/year (mpy)	in^2	5.34×10^5
mils/year (mpy)	cm^2	3.45×10^6
Milli meters/year (mmy)	cm^2	8.76×10^4

K = 3.45 x 1000000

Density: 7.8

Area: 4 cm2

Exposed time: 24 hr

1 mills /y = 0.0254 mm/y

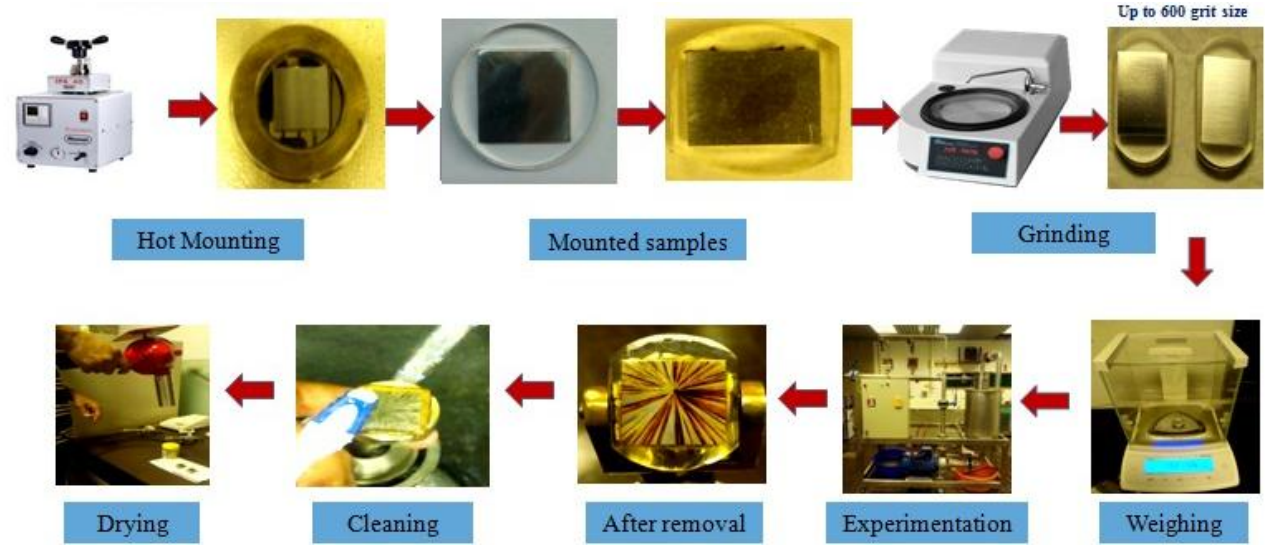

Figure 4. 8 Steps of one complete cycle in test procedure.

4.4 Methodology

Several test specimens from AISI 1030 and API X65 steels were prepared to study and compare their erosion corrosion behavior and mechanism. Each material was subjected to three different velocities 3m/s, 6m/s, & 12m/s at five different impingement angles from 15° to 90° in the test chamber. The impingement corrosion and erosion-corrosion rates at different impingement angles and under various jet velocities were measured for each material. A total of 120 experiments were carried out and later the surface morphology of eroded-corroded samples was characterized using scanning electron microscope to study the mechanism and material degradation. Experimental data was used to develop impingement erosion-corrosion correlations and these correlations will be later used to develop a prediction model.

CHAPTER 5

RESULTS AND DISCUSSION (Part 1)

5.1 Impingement Erosion Corrosion Behavior of AISI 1030 Steel

5.1.1 Effect of Impingement Angle

Erosion corroison rate depends on impingement angle on which the jet strikes the target material. Finnie et al. [15], describes that ductile materials like metals and alloys exibit a peak erosion rate at intermediate impingement angles e.g. 15°, 30°. However the peak eroiosn rate of a brittle material is observed usually at higher impingement angle i.e. 90° such as for glass material.

However, Burstein at al. [38], reported the peak slurry erosion rate occurs at intermediate angles, between 40° and 50°. At lower impingement angles such as 20° and 30°, the erosion rates were compareable to those observed at higher impact angle. The average affected area produced by impingement erosion corrosion was decreased with decreasing impingement angle. They reported that scars were shallower and elongated in the direction of the particle motion. So at lower angles erosion weight loss was less as compared to intermediate angles. The inconsistency in the erosion-corrosion behaviour could be because of different carrier fluids.

Furthermore, Fuyan et al. [19], explained that the difference in erosion pattern between slurry erosion and gas solid particle erosion must be associated with difference experimental conditions, carrier fluid which was carrying the impingement particles. Mostly the carrier fluid is the gas and liquid. Both of these fluids have a different

viscosities. The viscosity of water is about 100 times that of air. Hence at more oblique angle particles can penetrate deep in to the surface in case of air medium.

Figure 5.1 shows the effect of impingement angle on the impingement corrosion behavior of the AISI 1030 carbon steel in 0.2 molar NaCl fluid jet without solid particles at impact velocities of 3m/s. It is clear from the Fig 5.1 that the maximum impingement corrosion rate comes between 40° and 50° impingement angles, which is a typical behavior of ductile material. When the fluid moves radially on the surface the two stresses namely: shearing stress and normal impact stress impart their effect to determine the erosion corrosion wear rate as a function of impingement angle. In result of these stresses the deterioration rate was changed as a function of impingement angles. It could be explained that at lower impingement angles the shearing stress was dominating over impact stress whereas at higher impact angles the mechanical impact stress was dominant. However at 45º angle there is a balance between these two stresses and hence there is the maximum impingement corrosion rate at this intermediate angle. Y. Frank et al. [57], discussed the dependence of impingement corrosion rate on angle. He explained that there is a combined effect of shear stress and the normal impact stress developed on the surface of the target material in a result of fluid flow at certain angle and velocity. He determined that the maximum EC rate of the steel comes out at about 45° of the impact angle.

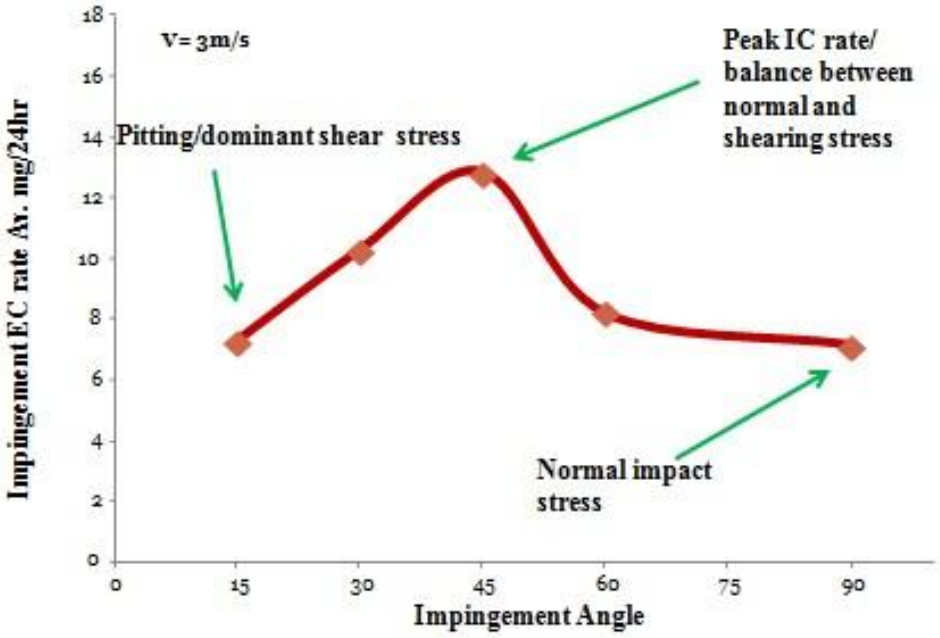

Figure 5.1 Effect of impingement angle on impingement corrosion rate of AISI 1030 carbon steel (without solid particle).

5.1.2 Effect of Fluid Jet Velocity

The impingement corrosion rate is related to the velocity of impinging jet. The correlation between impingement corrosion rate and velocity is generally reported as $E = K(V)^n$, where E is the erosion rate, K is the material constant that depends on particle size and impact angle. V is the fluid velocity, and n is the velocity exponent. The value of n is around 2 [58]. The effect of impingement velocity on impingement corrosion behavior of AISI 1030 mild steel is given in Fig 5.2 and values are mentioned in table 5.1. As expected, there is a large increase in impingement corrosion rate with an increase in impact velocity. This is attributed to the shear stress and normal stress on the wall surface of material. It is expected that the wall shear stress acting on the surface of the tested specimen increases rapidly with increasing flow velocity of the fluid. In particular when velocity is increased from 3m/s, 6 m/s to 12 m/s the shear stress is increased. Y Frank et al. [57] describes that at oblique angles i.e. 15º and 30º shear stress is maximum, whereas at higher angle the shear stress is minimum and impact stress is maximum at that high angle i.e. 90º, as shown in Fig 5.3 (a). Also it is demonstrated in Fig 5.3 (b) the fluid jet velocity is changed radially on the surface as a function of angle. At higher angles most of the energy of jet is utilized in the impact stress, hence the fluid flows with minimum velocity on the surface at higher angles. However, at lower angles fluid flows radially with its maximum velocity having more shear stress energy. As a result of increased shear stress with increase in velocity the impingement corrosion rate was also increased. As the impingement corrosion rate was increasing the mass transfer rate from the surface of the sample was increased. This is one of the factors that contribute in higher impingement corrosion rate by increasing the jet velocity. It is observed during

experiment that there is continuous removal of the corrosion product from the surface by the fluid movement. However increasing the velocity also increases the mass transport of oxygen to the surface as discussed by Liu et al. [59]. Furthermore, as shown in Fig 5.4, it is observed that as the fluid impinged and flows radially on the surface with a certain velocity. The recessed scars having gaps between them were formed in the direction of fluid movement. Close to the impingement point there are high velocity regions on the surface, which are analyzed by optical profilometery and FE-SEM analysis.

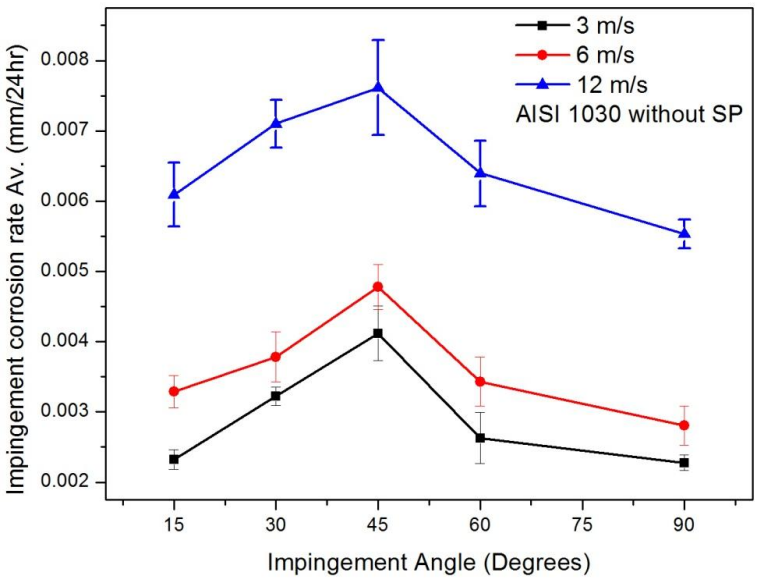

Figure 5. 2 Effect of impact velocity/angle on impingement EC rate of AISI 1030 steel without solid particle

Table 5. 1 Impingement Corrosion Rate as a Function of Angle and Velocity

Impingement Corrosion Rate, AISI 1030 (Average, mm/24hr) Without SP						
Impingement Angle		15	30	45	60	90
Jet Velocity	3m/s	0.0023	0.0032	0.0041	0.0026	0.0022
	6m/s	0.0032	0.0037	0.0047	0.0034	0.0028
	12m/s	0.0060	0.0071	0.0076	0.0063	0.0055

(a)

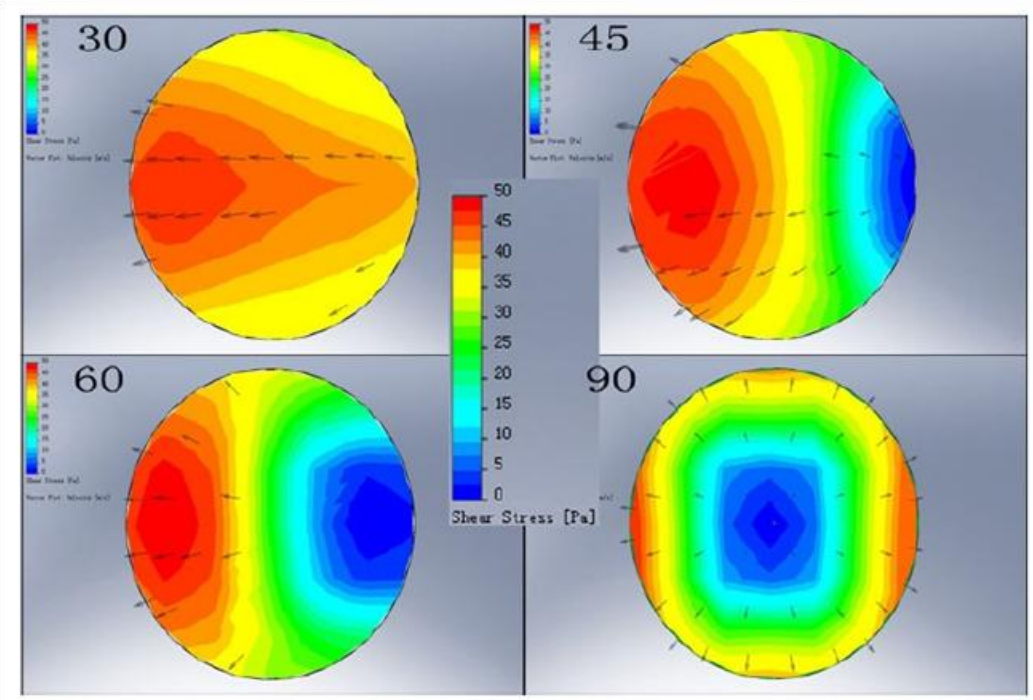

(b)

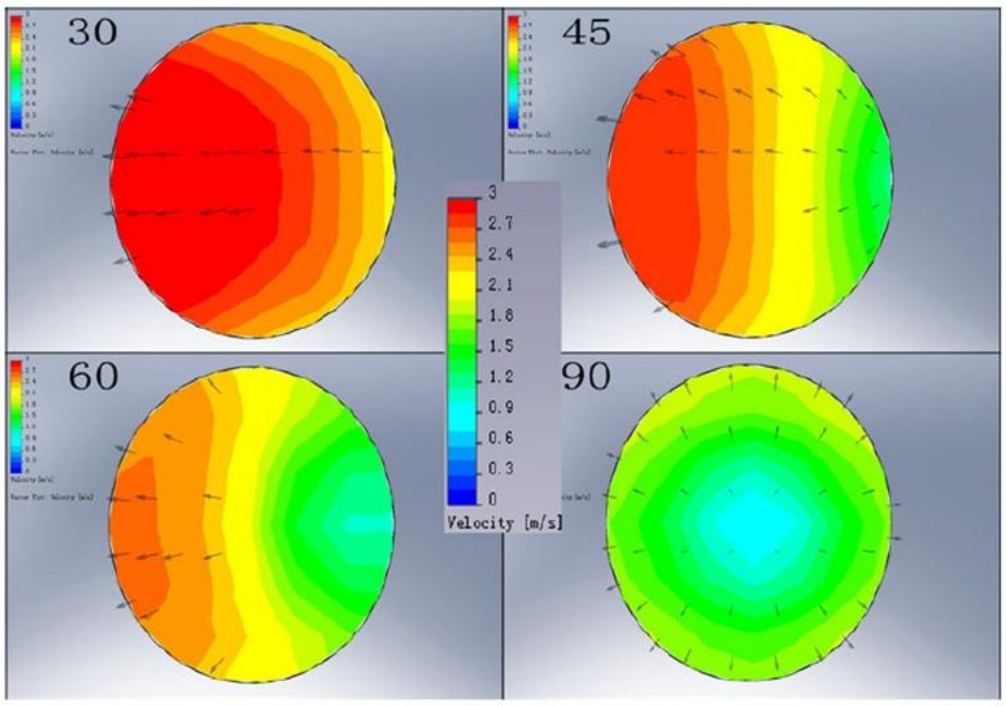

Figure 5.3 (a) Distribution of shear stress, (b) Distribution of fluid field on the steel surface [54].

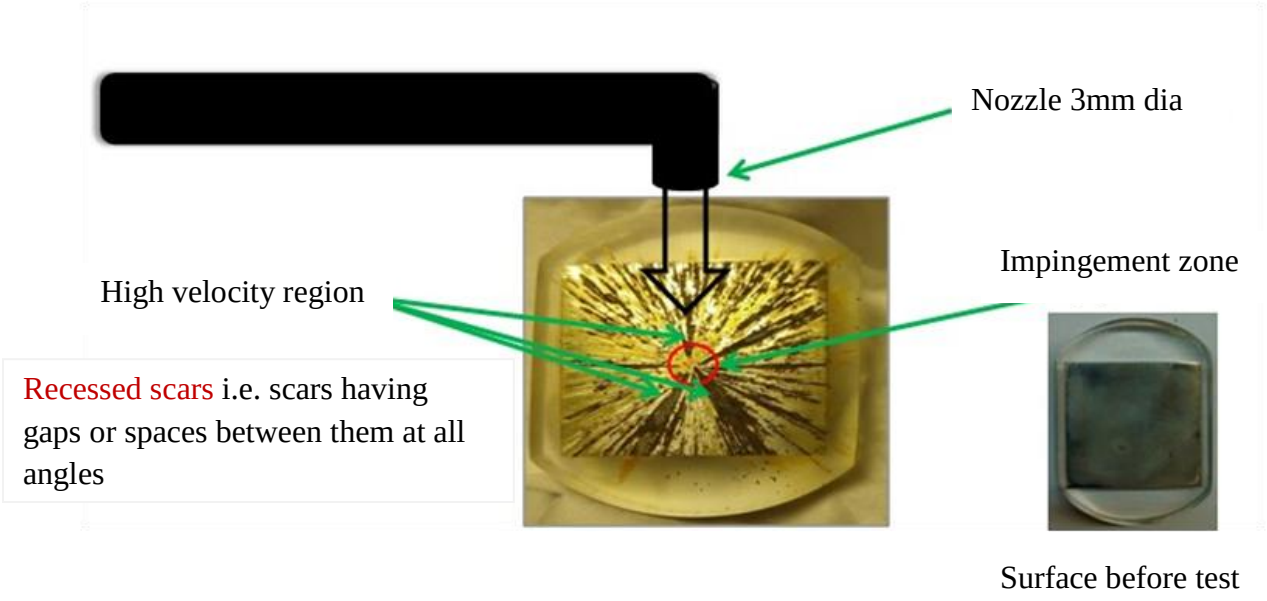

Figure 5. 4 Impingement Corrosion patterns and high velocity regions.

5.1.3 Surface Morphology and Wear Scar Features

Figure 5.5 (a-e) shows SEM images of AISI 1030 carbon steel after impingement corrosion without solid particles at five impact angles from 15° to 90°. we observed number of scars and their morphologies on the surface at different angles. Impingement corrosion scars have different patterns and depth as verified by the optical profilometery. The scar depth is the distance from the deepest point within the damaged zone to the unaffected surface of the specimen which acts as a reference plane. In Figure 5.5 (a-e), shows different shapes of the impact point area, where fluid jet first hits on the surface. This impact shape we observed during test which depicts that at lower angle impingement point was more elliptical. However, as we increased the angle from 15°-90°, less elliptical shape was there and it becomes circular at a maximum angle of 90°

degree. This is one of the evidence of the change in effect of shearing stress at oblique angles to impact stress at higher angle. At the impact point, as shown in FE-SEM images, these points are unaffected because of the possible stagnation zone. Also at lower impact angle of 15° as the fluid impacted on the surface, it flows radially on the surface approximately uniformly all over the surface with less drop in jet velocity. It is observed that at lower angle like 15°, the shearing component of the fluid is maximum as described in above section. Furthermore the wear scars are neither continuous nor they are much deeper as compared to angle in between 40° and 50°. Shallow pitting is more at lowest angle all over the surface. Because of the domination of the shearing component over normal impact component, rougher surface is generated at lower angle e.g. 15°. Inclusions can be exposed to the aggressive solution on the larger bare metal surface, leading to a greater probability of generating pits [38]. However in Fig 5.5 (b-e), it is observed that scars generated at 30° angle were wider, deeper and continuous as compared to 15° angle. This is due to the normal stress component, which came into play with increasing impingement angle. Whereas, at 45° impact angle the number of scar and total effected area is greater as compared to the lower and higher impact angles. It was observed that they are continuous towards the boundary of the specimen. As it is expected a balanced effect of the two stresses, which resulted in the highest impingement corrosion rate at about 45°. By increasing angle after 45° the normal impact component becoming dominant and it can be observed in SEM image Fig 5.5 (d). At 60° impingement angle the wear scars are less in number and it is observed that these are shallower scars. Furthermore at 90° impact angle the normal component is maximum also after the impact the fluid does not have much energy to erode the surface deeper and

imprint number of scars as it is observed in case of 45°. The wear scars and their penetration depths were examined and verified by A GTK-A 3D optical profiler from Bruker Co.

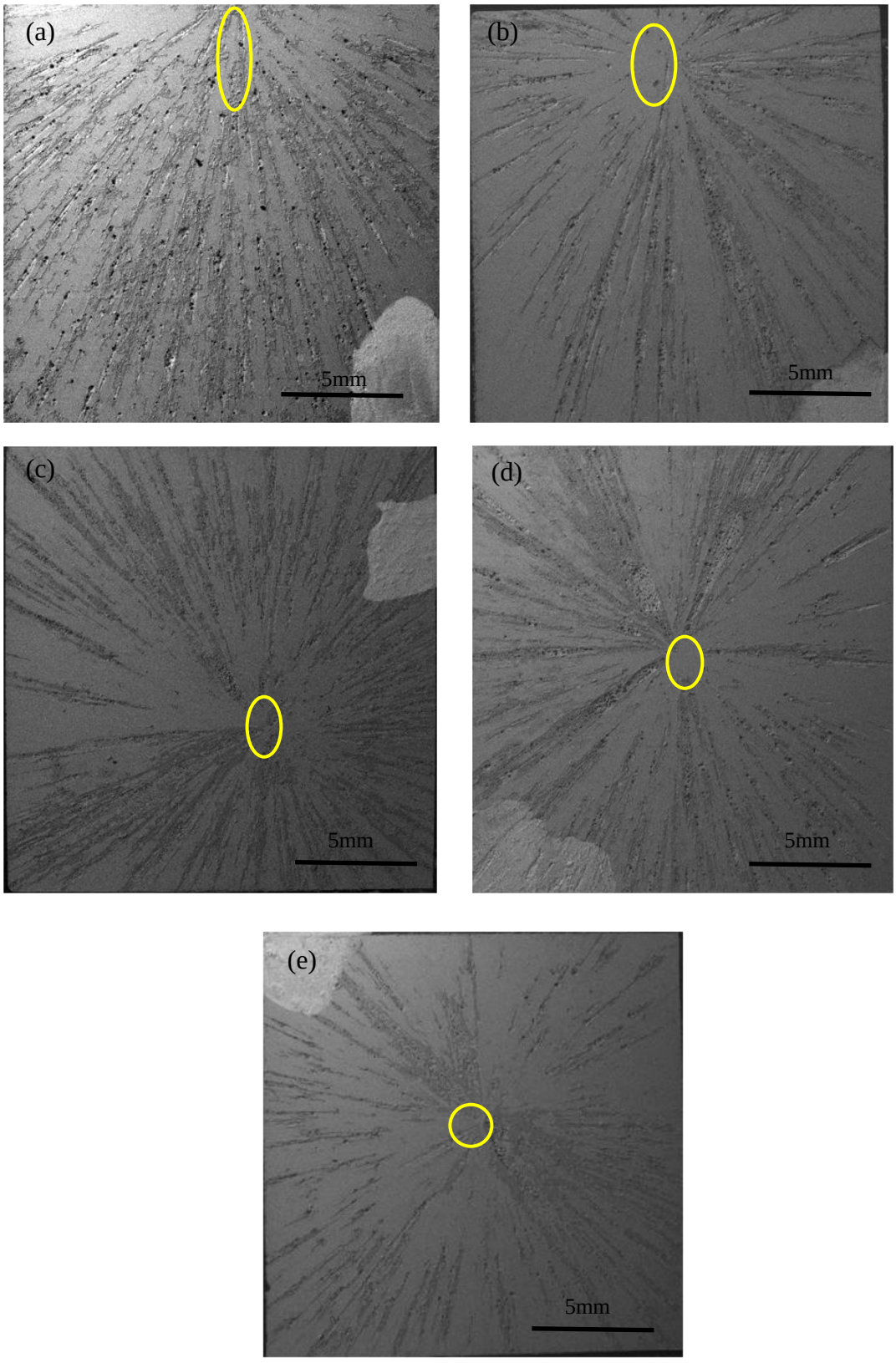

Figure 5. 5 FESEM images (a to e angles 15-90 respectively) shows wear scars and morphology after experimentation.

5.1.4 Impingement Erosion Corrosion Behavior of AISI 1030 Steel

During erosion corrosion the vertical component of the kinetic energy of the impinging jet is consumed to penetrate particle in to the material while horizontal component of kinetic energy is used in the ploughing of the material as the abrasive particle slides on the surface. Fig 5.6 shows that, as we increased the velocity the kinetic energy increased and in result of that there is an increase in material loss (table 5.2). At oblique angles i.e. 15° and 30° the horizontal component is higher than the vertical or indenting component of the kinetic energy, hence we found the elongated ploughing and longer erosive track and abrasive particles come in contact with more surface area as compared to higher impact angles. Also because of the shearing stress, sand particles plastically deform the surface and cause erosive tracks with raised lips on the surface, along with elongated sliding as shown in Fig 5.7 (a-b).

Whereas as we increase the impact angle after 45° angle the indenting component of the kinetic energy becomes greater than the horizontal component and flattening and fracture of the platelets dominated over ploughing. At high impact angle i.e. 90°, most of the kinetic energy of the particles is utilized in the penetration of the surface, forms dimples and craters. Ridges that formed around the dimples were flattened by the impacts of the subsequent particles, which are then removed by the fracture due to the plastic deformation and repeated impacts by the incoming particle stream. We found the mechanism of formation, extension and subsequent breaking of the highly distressed platelets, the higher the impact velocity, deeper the particles penetrate and more material is removed. This metal removal process is dominated under conditions of the high impact velocity and high impact angles as shown in Fig 5.7 (e-f) [60]. Also we found that at 90º

angle there is slight increase in material loss. This is because of the slight increase in hardness value after multiple strikes of the sand particles and it was 308Hv (Average) after experiment.

However as we increased the impact angle to 45° degree, normal stress is also have a strong effect during impact of jet having silica sand particles, because of this normal component along with shearing stress component caused less sliding but deeper penetration Fig 5.7 (c-d) of sand particles into the surface and hence have larger raised lips along with shorter and deeper erosive impacts. It could be suggested that the balance between normal, tangential stress and shearing stress is the factor that enhances the erosion corrosion rates of carbon steel. This balance of optimum penetration and significant sliding of sand particles on the surface results in more raised lips and removal of the lips by subsequent particle impacts [61].

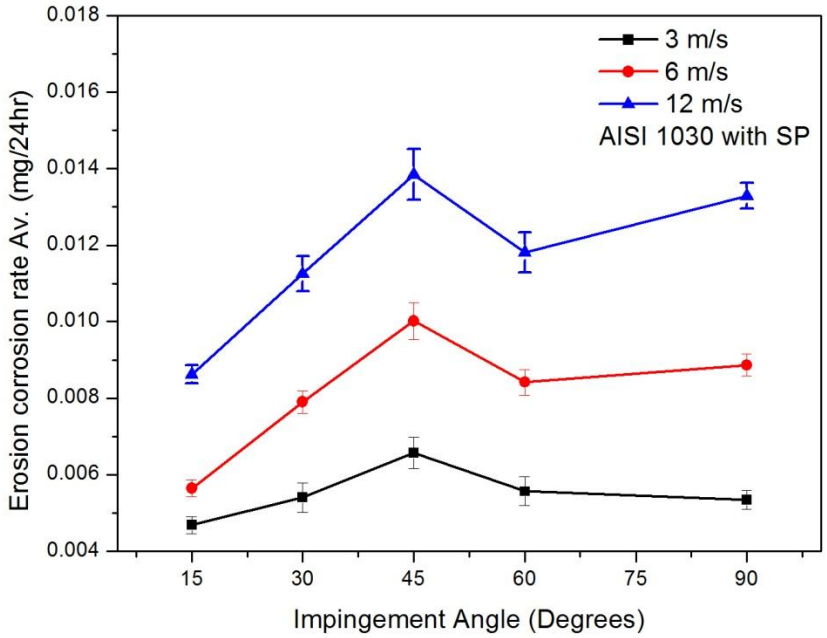

Figure 5. 6 Effect of impact velocity/angle on impingement EC rate of AISI 1030 steel with solid particle

Table 5. 2 Impingement Erosion Corrosion Rate as a Function of Angle and Velocity

Impingement Erosion Corrosion Rate , AISI 1030 (Average, mm/24hr) With SP						
Impingement Angle		15	30	45	60	90
Jet Velocity	3m/s	0.0046	0.0054	0.0065	0.0055	0.0053
	6m/s	0.0056	0.0079	0.010	0.0084	0.0088
	12m/s	0.0086	0.0112	0.0138	0.0118	0.0013

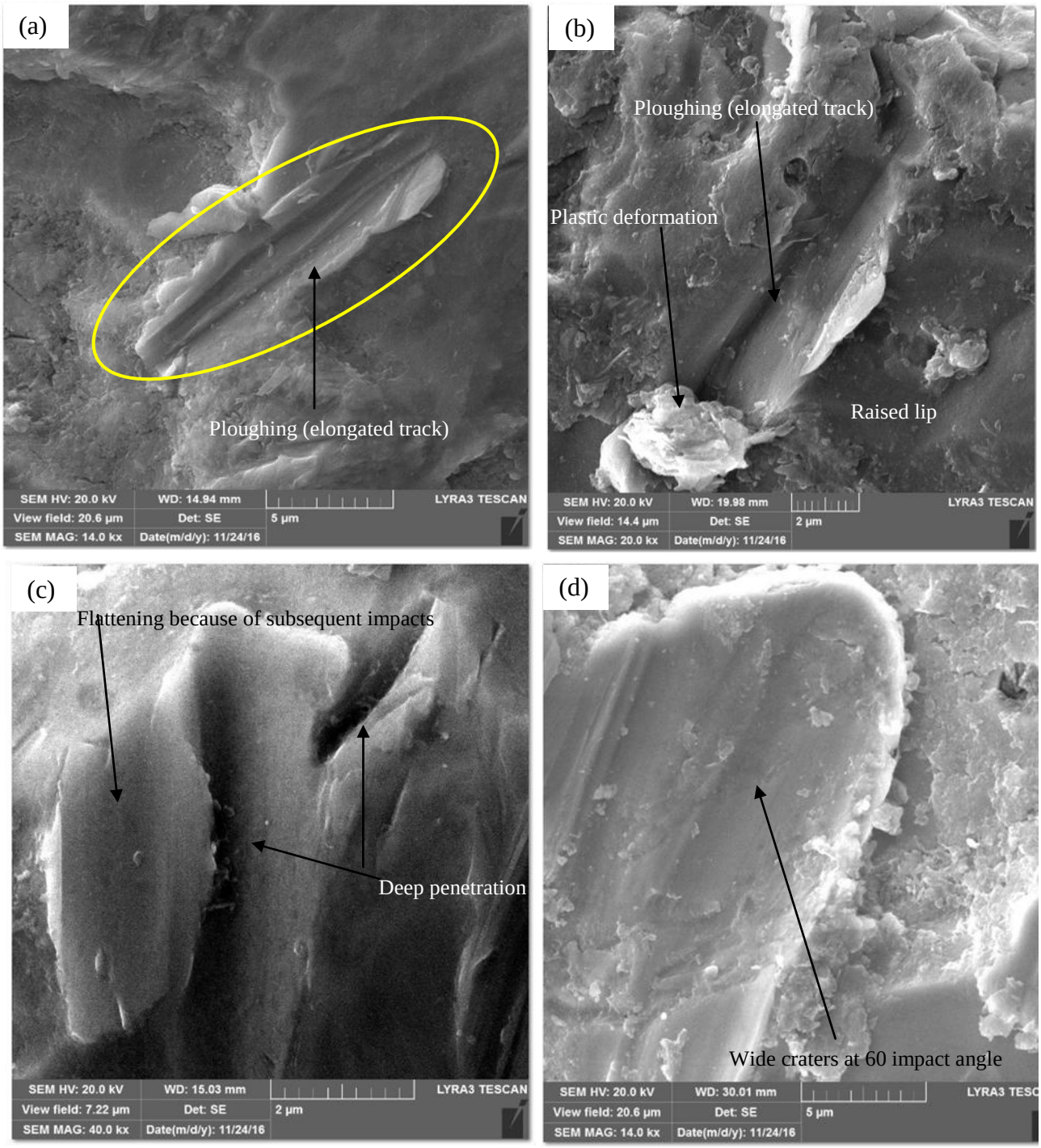
(a)
Ploughing (elongated track)
SEM HV: 20.0 kV
WD: 14.94 mm
LYRA3 TESCAN
View field: 20.6 µm
Det: SE
5 µm
SEM MAG: 14.0 kx
Date(m/d/y): 11/24/16
(b)
Ploughing (elongated track)
Plastic deformation
Raised lip
SEM HV: 20.0 kV
WD: 19.98 mm
LYRA3 TESCAN
View field: 14.4 µm
Det: SE
2 µm
SEM MAG: 20.0 kx
Date(m/d/y): 11/24/16
(c)
Flattening because of subsequent impacts
Deep penetration
SEM HV: 20.0 kV
WD: 15.03 mm
LYRA3 TESCAN
View field: 7.22 µm
Det: SE
2 µm
SEM MAG: 40.0 kx
Date(m/d/y): 11/24/16
(d)
Wide craters at 60 impact angle
SEM HV: 20.0 kV
WD: 30.01 mm
View field: 20.6 µm
Det: SE
5 µm
SEM MAG: 14.0 kx
Date(m/d/y): 11/24/16

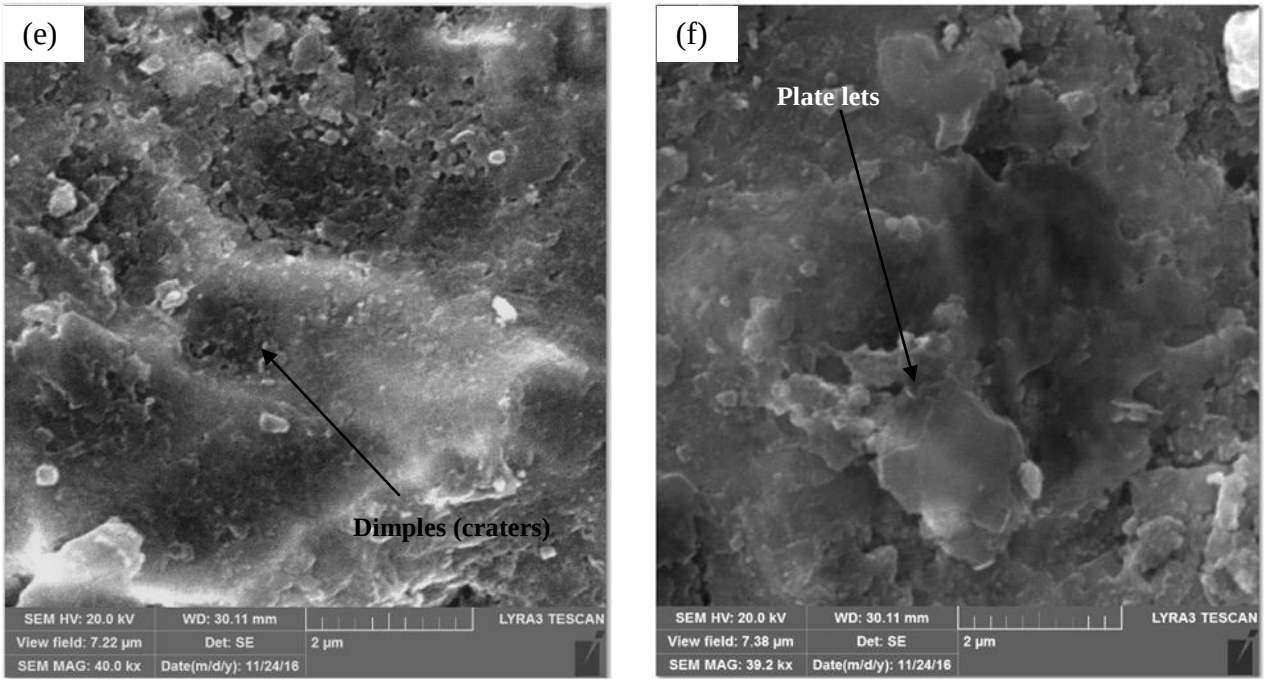

Figure 5. 7 SEM image (a-d, angle 15-60 respectively and e-f Angle 90) shows different mechanism of material removal.

5.1.5 Correlation with Erosion Corrosion Model

It is very useful to simulate to predict the erosion corrosion behavior of materials under consideration environment in the form of correlations. Prediction models are expressed generally as a function of velocity, impingement angle, particle size and shape, target material properties. Most famous models are those presented by Finnie [62, 63], Sundararajan [52] and hutching [51]. Model that is presented by Finnie and recently utilized by Xianghui Chen [64] at university of Tulsa erosion corrosion research group for carbon steel is as given below.

$$\mathrm{ER} = AF_s V^n f(\theta) \qquad \text{eq (2)}$$

Where ER is the erosion rate (mg/mg), A is an empirical constant, V is the particle impingement velocity, and n is an empirical coefficient. In research at erosion corrosion research centre of university of Tulsa demonstrated that a value of n is equal to 1.73 and that is fit to utilizing for various oilfield materials. F_s is a particle shape coefficient, Fs = 1.0 for angular sand particles. While f theta is the function of the impact angle that is given in below equation.

$$f(\theta) = x\cos^2\theta\sin(w\theta) + y\sin^2\theta + z \qquad \text{eq (3)}$$

Whereas w, x, y, and z are empirical constants that depend on the material being eroded. The suitable values of the model constants, assuming V has units of ft/s, are provided by for carbon steel [64]. In the present work, the experimental data was correlated with

above mentioned model and values of A and z were determined by performing regression analysis using MATLAB software. Lower and upper bounds for A are 0.012 and 0.0396 whereas for z are 0.428 and 0.572 respectively. Values of the correlation coefficient $R^2 >$ 98.8% indicating a good fit using the given parameters [64]. Furthermore, using known parameters mentioned above, erosion rates were calculated at v = 12 m/s for impingement angles ranging from 15° to 90°. A comparison between the experimental erosion rate curves with those calculated using Finnie model is shown in Fig 5.8. The calculated erosion rate indicates a good agreement with the present experimental data of AISI-1030 carbon steel. Consequently, the model of Finnie can be used to determine the erosion corrosion rate with reasonable accuracy. However, the parameters for this model given and calculated are specific to current test materials and test conditions.

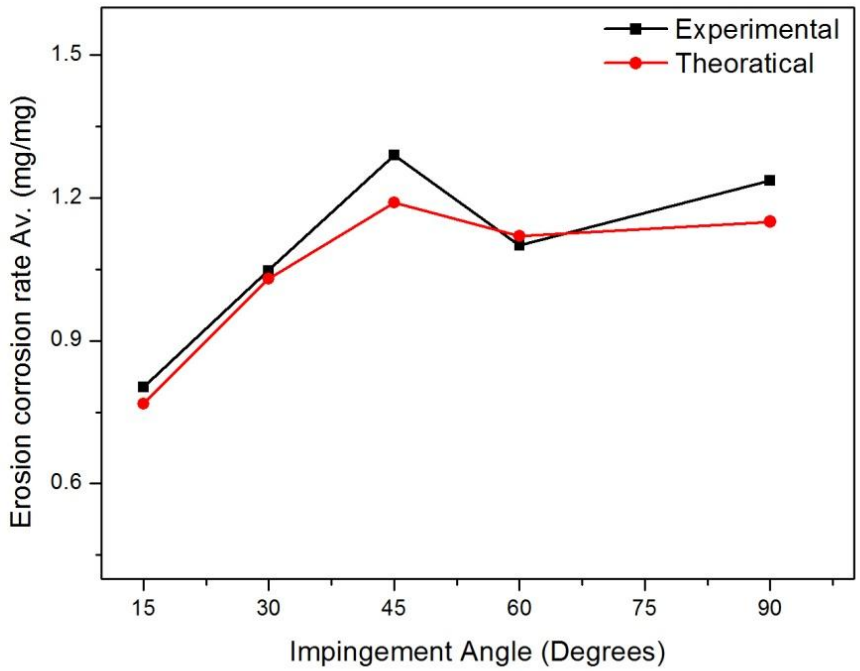

Figure 5.8 Comparison of experimental and Finnie et al. model curve fitting erosion-corrosion rate curves for carbon steel AISI 1030

5.1.6 Effect of Erosion on Corrosion

Figure 5.9 shows, that the impingement erosion-corrosion has a significant effect on material loss because of the effect of erosion on corrosion at all impingement angles. This reveals that the introduction of solid particles intensify the erosion corrosion mechanism of AISI 1030 steel at all impingement angles. This results in more severe degradation in impingement erosion corrosion experiments as compared to impingement corrosion i.e. without solid particles. In case of AISI 1030 steel, it is clear from the graph that the synergistic effect at 45° and 90° angle is more as compared to other angles. At 45° there is deep penetration of particles because of combined effect of shear and impact stress. This accelerates the impingement corrosion in result of surface activation as shown in Fig 5.10 (a-b). Also at 90° impact angle due to extensive extrusion and fracture of platelets, erosion enhances corrosion significantly. We considered impingement corrosion rates as pure corrosion damage; however by introducing solid particles we have total damage of erosion and corrosion. Hence the synergistic i.e. the effect of erosion on corrosion is obtained by subtracting the impingement corrosion values from total material loss in results of impingement erosion-corrosion by solid particles, equation is shown as below.

$$\text{Total Impigement EC} = \text{Impingement Corrosion} + \text{Impingement Erosion} \qquad \text{eq (4)}$$

In previous studies it is shown that by introduction of solid particles, the cutting mechanism is dominant on the surface of target material. It is clear from the erosion corrosion results that introduction of solid particles are responsible for the increase in material loss. As the surface roughness increases, localized attack accelerates, hence there is close link between particles contact force exerted on a surface and predicted material

degradation rate [65]. Furthermore there is no evidence found in EDX analysis for sand particles remain at 90 º embedded in the surface as shown in Fig 5.11.

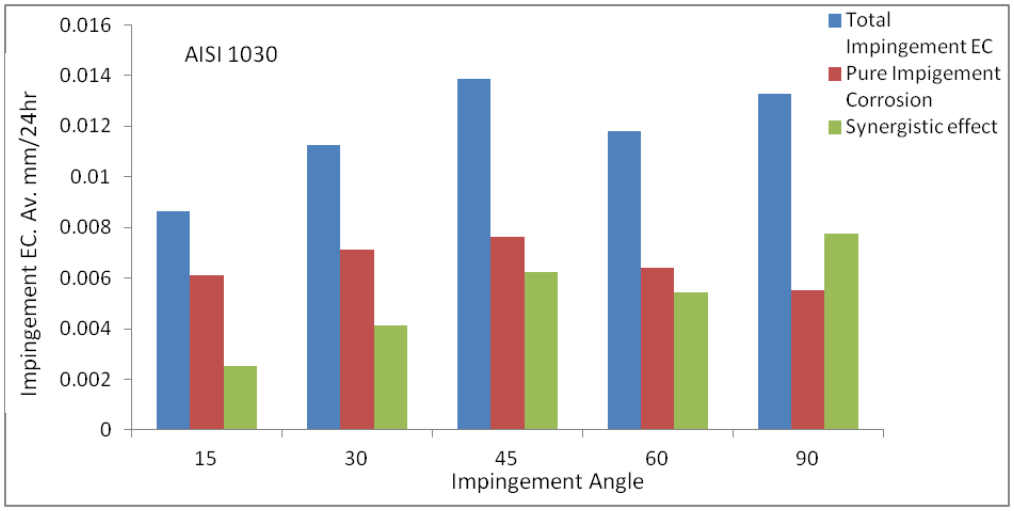

Figure 5.10 Effect of erosion on corrosion rate with the introduction of sand particles.

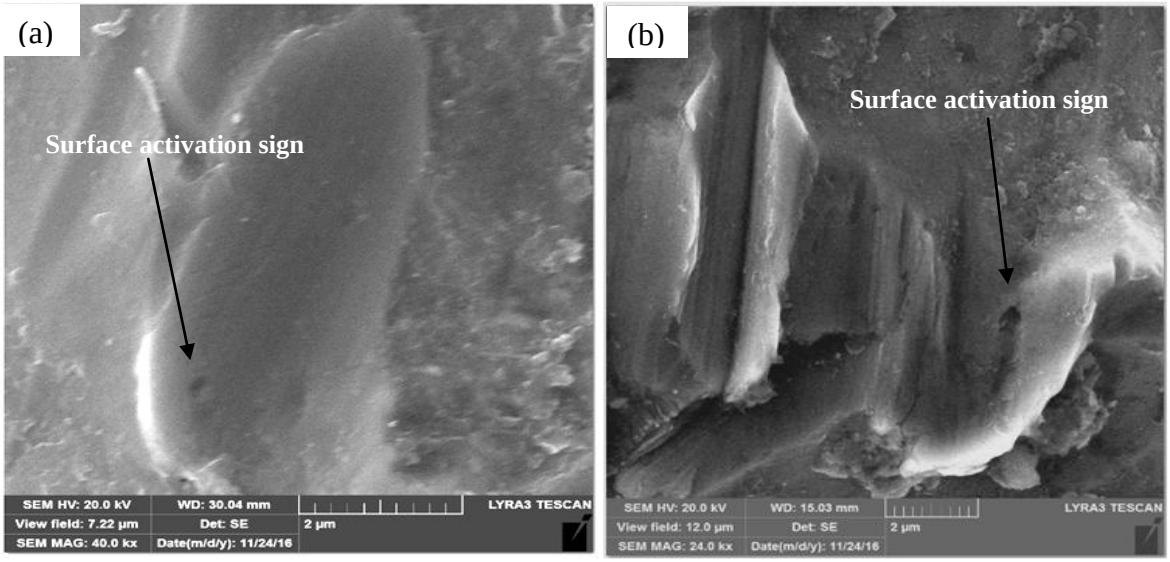

Figure 5.9 FESEM image shows surface activation and effects of erosion on corrosion; (a) 60° (b) 45°.

(a)

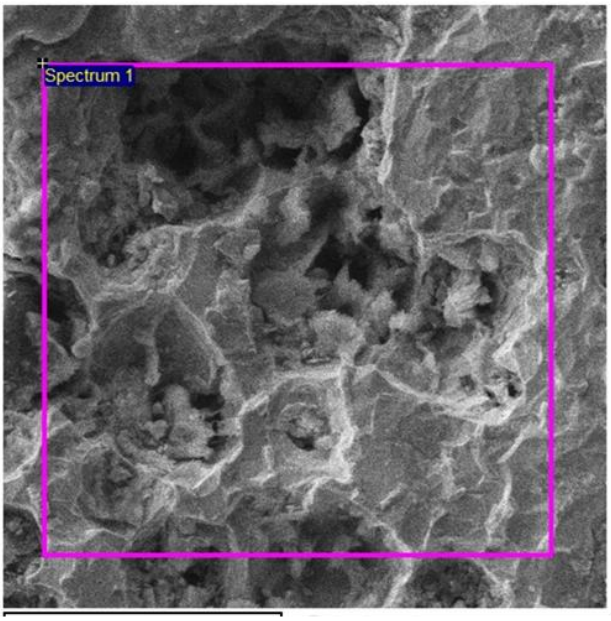

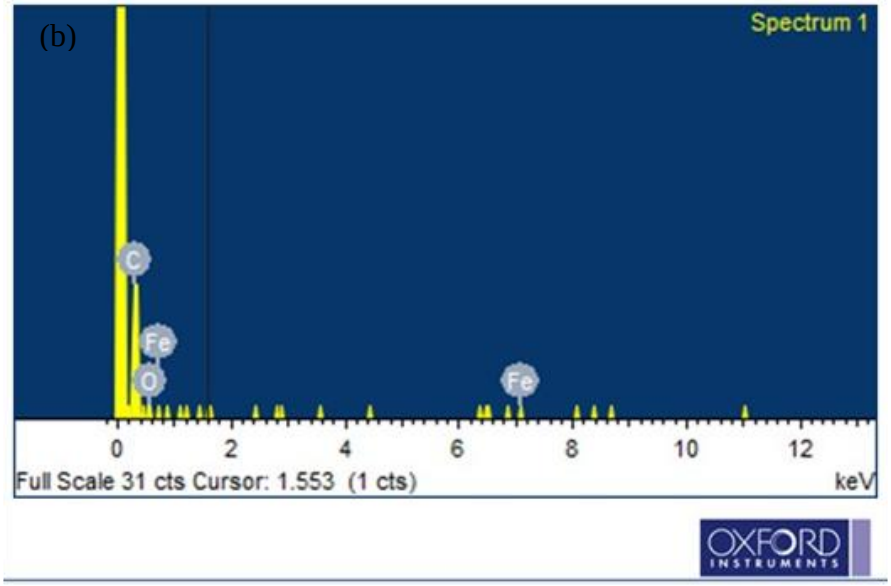

Figure 5.11 EDX Analysis of tested sample AISI 1030 Steel at 90º in presence of solid particles.

5.1.7 Investigation of the Wear Scars Using Optical Profilometer

As shown in Fig 5.4 there are high velocity regions near the impingement point. We are expecting the maximum effect of shearing stress or normal impact stress in this region. We examined the maximum depth (average) of the wear scars that are produced after experimentation at 12 m/s velocity for 24 hrs at 15° - 90° angles in-case of impingement corrosion and impingement erosion-corrosion (table 5.3). Typical 3D image analysis of wear scars and their penetration depths examined and verified by A GTK-A 3D optical profiler from Bruker Co. Effect of shear stress and impact stress could be examined from the results of 3D profiles of regions near the impingement points where we are expecting maximum depths. It was found during impingement corrosion (without solid particles) as we increase the angle up to 45° degree the penetration depth becomes maximum i.e. 40 ± 5µm, Fig 5.12. It is because of the balance between the shear stress and normal stress, which resulted in significant material removal. It is discussed by other researchers that the maximum depth varies by the shear stress [65, 66]. It is demonstrated in Fig 5.13 that wear depth is a function of the shear stress, normal stress and the solid particle erosion effect on corrosion. However, with the introduction of solid particles it is clear that the particle ploughed deeper (as discussed in earlier sections) at intermediate angle i.e. 45° degree giving 57 ± 5 µm depth. Whereas, at 90° angle maximum kinetic energy of the particles utilized in strike which activates the surface by extrusion and form platelets. These were then fractured and removed by the subsequent impact of the particles. Hence as shown in 3D image Fig 5.14 (e) the affected area at impingement point also eroded and recessed scars becomes wider. Maximum depth at 90° angle was 38 ± 3 µm in case of solid particles.

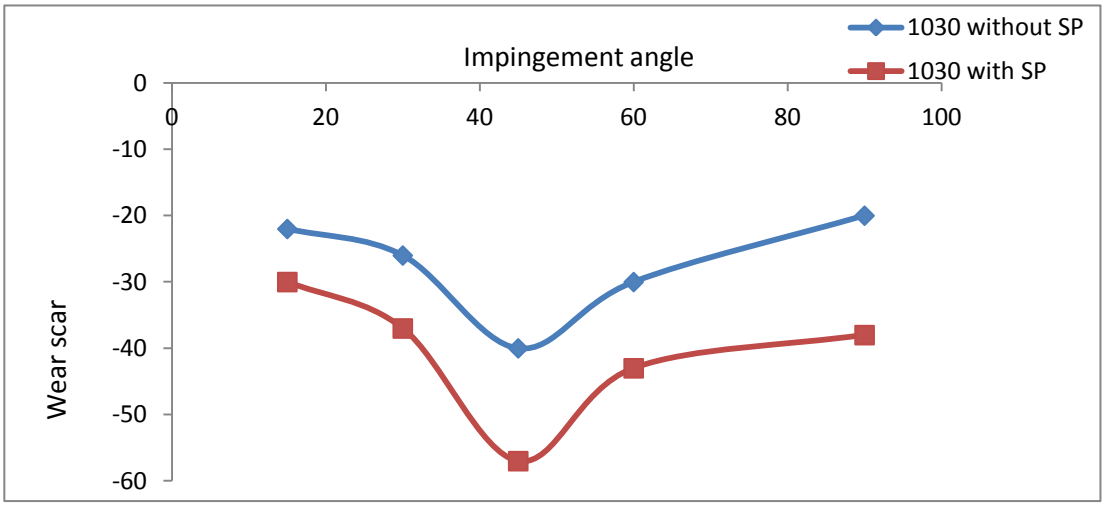

Figure 5. 12 Trend of the Wear scar penetration depth in microns.

Table 5. 3 Average Scar Depth Values (AISI 1030 Steel)

Impingement Angle	15	30	45	60	90
Wear Scar Depth (µm) AISI 1030Steel (without SP)	22	26	40	30	20
Wear Scar Depth (µm) AISI 1030Steel (with SP)	30	37	57	43	38

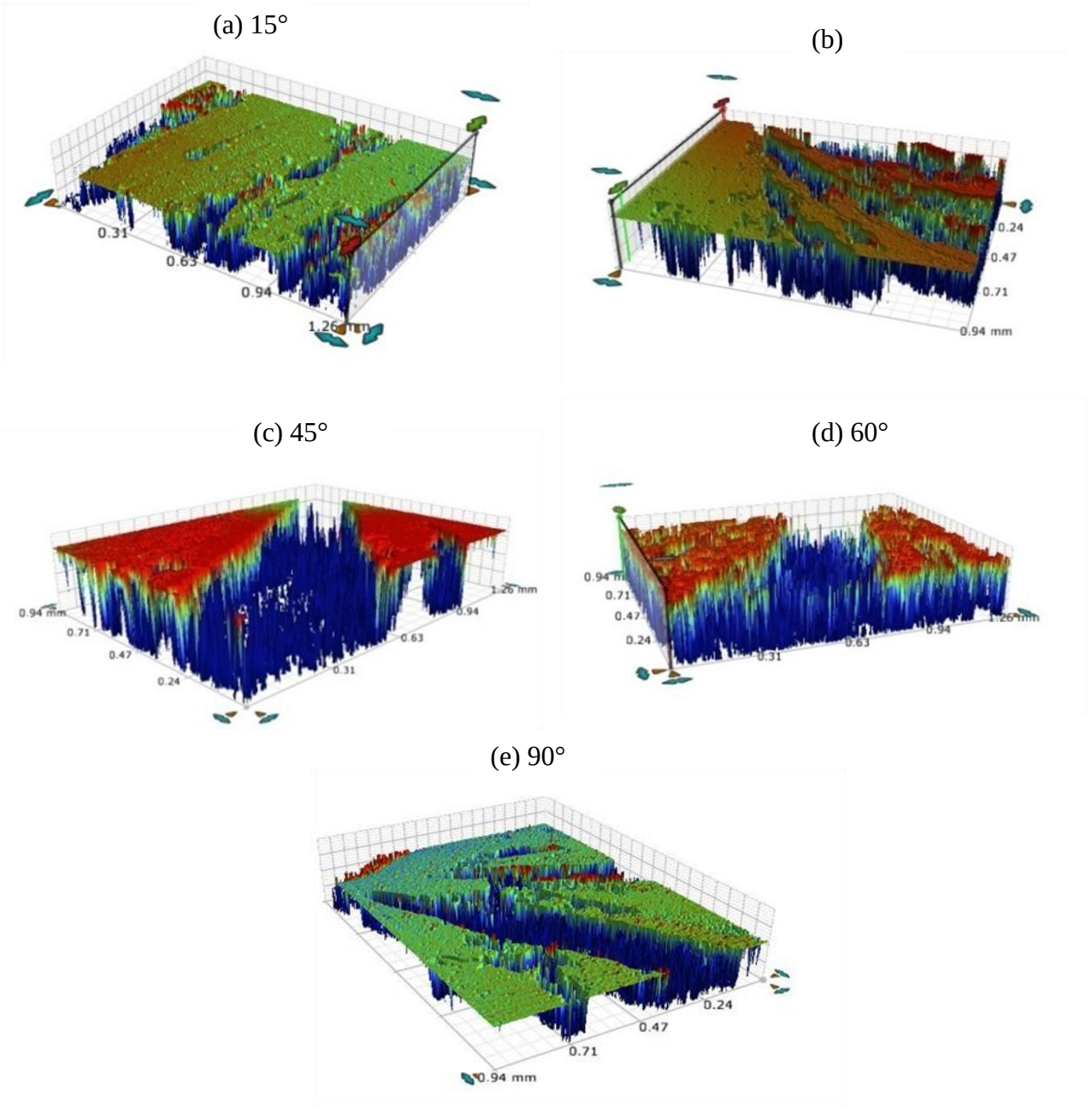

Figure 5. 13 Optical images near high velocity regions in absense of solid particles

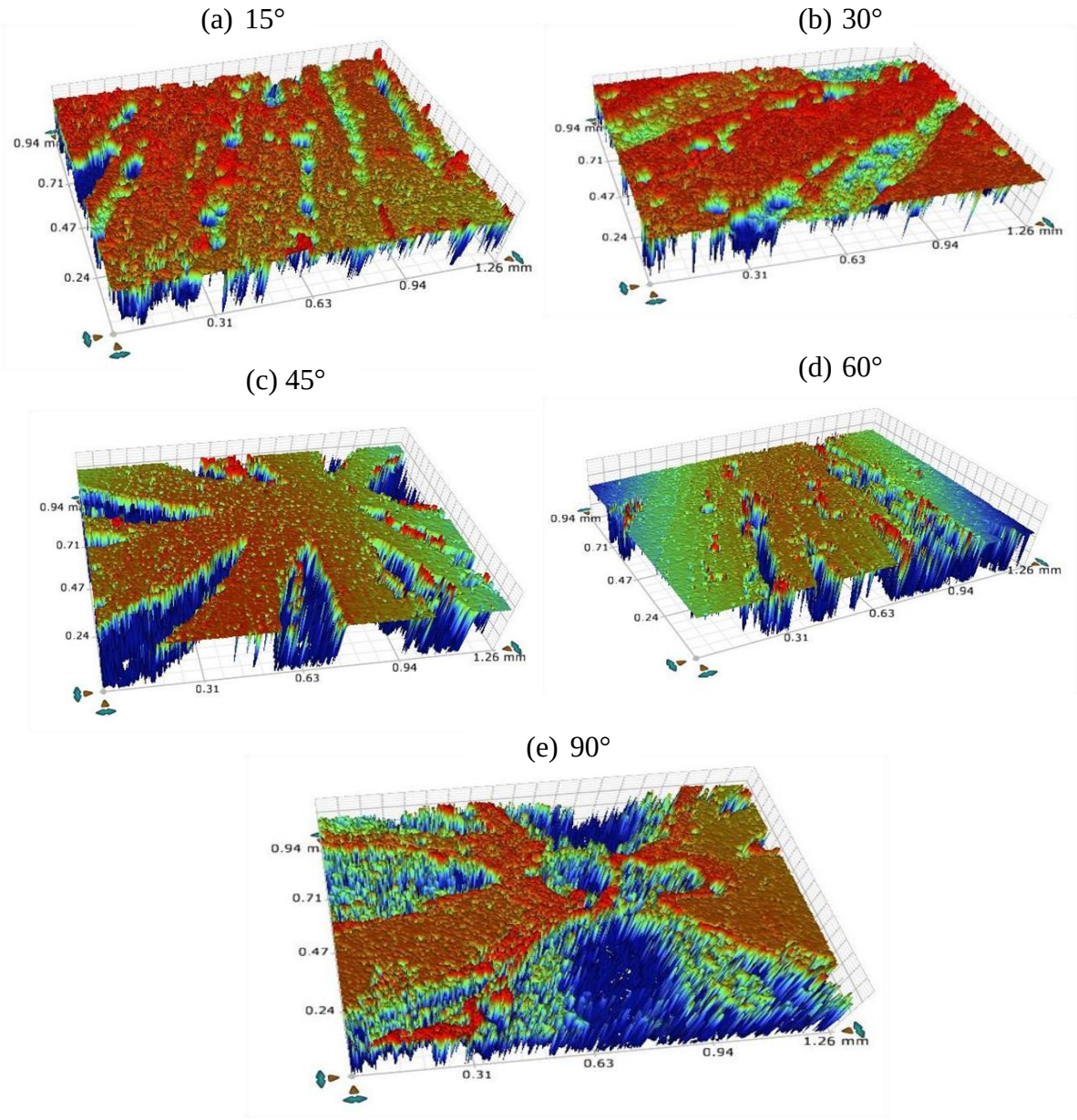

Figure 5. 14 Optical images near high velocity regions in presence of solid particles

5.2 Impingement Erosion Corrosion Behavior of API 5L X65 Steel

5.2.1 Effect of Impingement Angle and Velocity

The pure impingement corrosion rate of X65 carbon steel as a function of impingement angle is shown in Fig 5.15 and values are given in table 5.4. It is clear that the maximum and minimum impingement corrosion comes at impingement angle of 45° and 90° respectively. The presence of plate like circular holes at lower angles depicts that, corrosive slurry has passed through the surface and attacked target surface. At oblique angles like 15° and 30° fluid flow radially having its maximum velocity. Forming a stagnation layer of fluid over the larger surface area because of the high velocity with which fluid moves. This promotes the susceptibility of the localized reaction. Furthermore fluid movement provides reacting species (chlorides ions) to the activated or inclusion sites [67]. The greater susceptibility of pitting under oblique impact is due primarily to larger bare metal surface generated by the fluid on the surface. As explained in previous section 5.1, It was found that in impingement corrosion, there is the stagnation layer formed directly at impingement point. Whereas, at higher angle and in presence of solid particles central region was also eroded. It was found that wear scars or patterns have gaps among each other in the direction of the fluid. The impingement points, showed elliptical to circular morphology, which is due to the fact that tangential force or shearing stress is maximum at lower angles, while normal impact or extrusion force is maximum at higher angles. Hence it is observed that corrosive fluid caused pitting as well as recessed wear tracks in the direction of fluid. Formation of pits could be explained that, first corrosion product formed and electrolyte goes underlying surface which could results in localized stagnation condition in which it grows [50]. However

with the flow of fluid and shearing stress energy of the moving fluid these pits then elongated in to a wear track. Furthermore at 45°, the number of scars and total effected area is greater as compared to the lower and higher impact angle. It is clear from the Fig 5.16, that these scars are continuous towards the boundary of the specimen. As expected, a balanced effect of the two stresses resulted in the highest impingement corrosion rate at about 45° of the fluid impact. With increasing angle beyond 45° the normal impact component is becoming dominant as shown in Fig 5.16. whereas at 60° the wear scars are less in number and it is observed by optical profilometery that these are shallower scars. Furthermore at 90° impact angle the normal component is maximum and after the impact, fluid does not have much energy to erode the surface further and produce number of scars as it was observed in case of 45°. The wear scars penetration depths close to the impingement points were examined by optical profiler from Bruker Co.

As shown in Fig 5.15 as the velocity is increased impingement corrosion rate is also increased. The Impingement corrosion rate at 3 m/s and 6 m/s does not have much difference. However as we increased the velocity to 12 m/s corrosion rate was significantly increased. This is due to increase in stresses on the wall surface of material at higher velocity i.e. 12m/s. It expected usually that the wall shear stress acting on the surface of the tested specimen increases rapidly with increasing flow velocity of the impinging fluid jet. As a result of increased shear stress with an increase in velocity, the impingement corrosion rate was also increased. It was found in both type of steels, that during impingement corrosion tests corrosion product continuously removed from the surface with the flow of fluid. However some scale remained intact on the surface. Hence

the mass flow rate also increased with an increase in velocity of impinging jet, which resulted in an increase in mass loss with velocity.

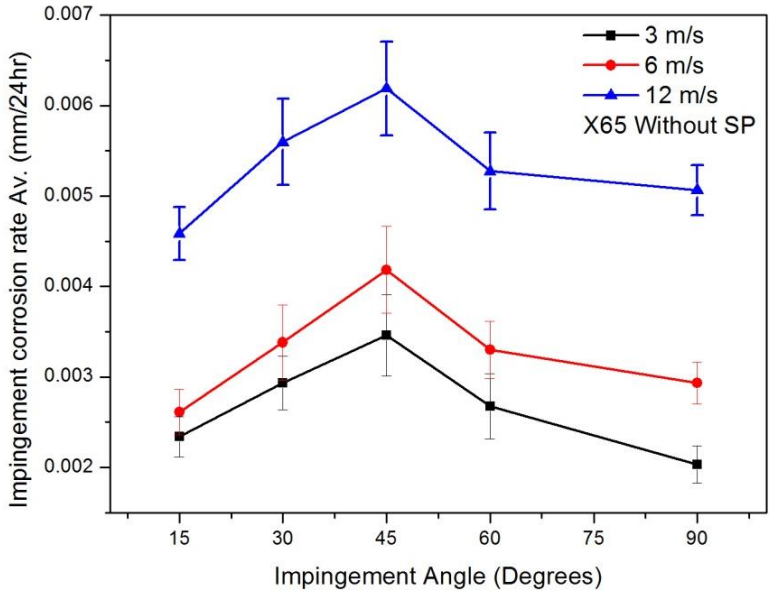

Figure 5. 15 Impingement corrosion rate as a function of angles at 3 different velocities

Table 5. 4 Impingement Corrosion Rate as a Function of Angle and Velocity

Impingement Erosion Corrosion Rate, API X65 (Average, mm/24hr) Without SP						
Impingement Angle		15	30	45	60	90
Jet Velocity	3m/s	0.0023	0.0029	0.0034	0.0026	0.0020
	6m/s	0.0026	0.0033	0.0041	0.0033	0.0029
	12m/s	0.0045	0.0055	0.0061	0.0052	0.0050

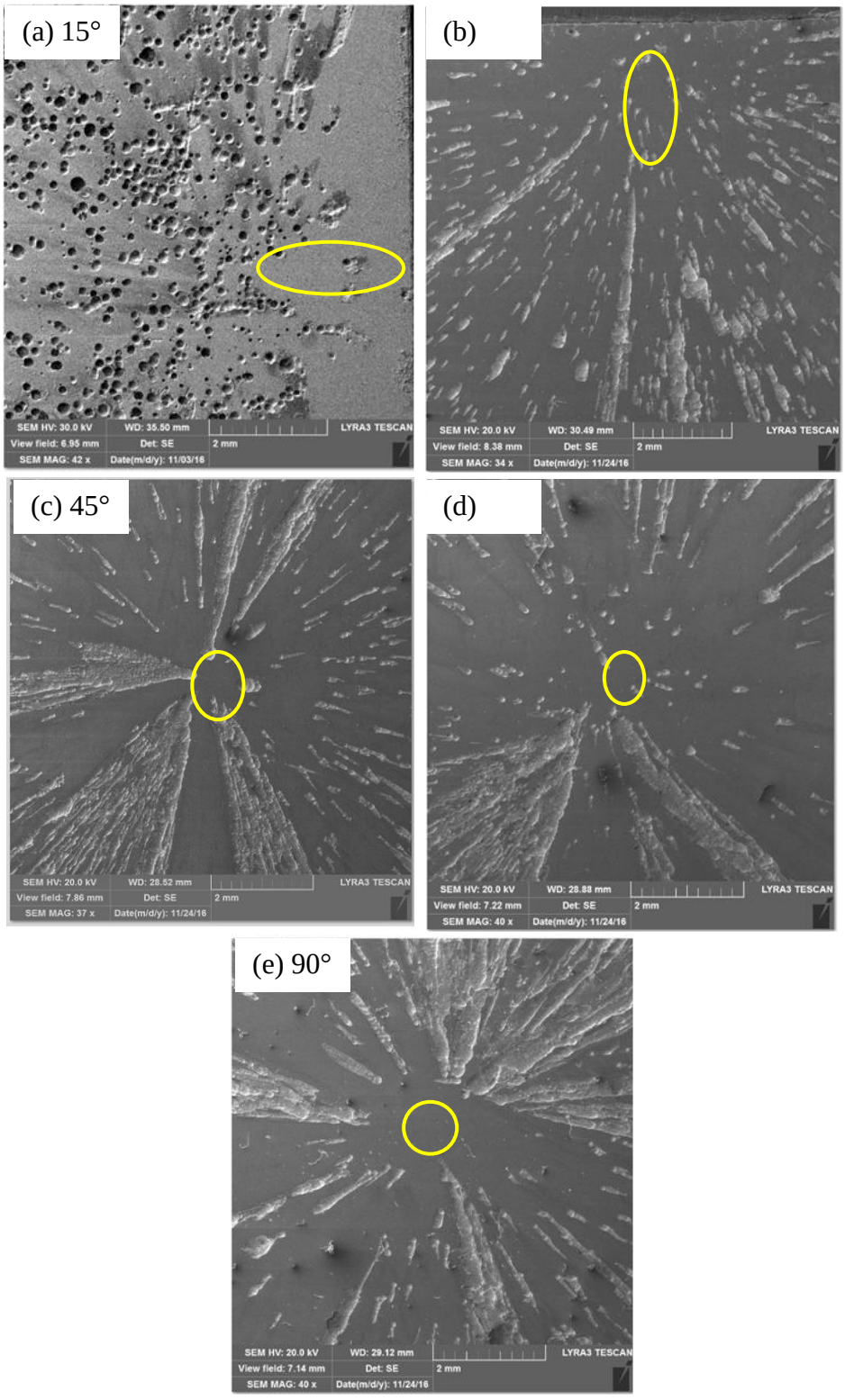

Figure 5.16 FESEM images shows the wear tracks and different morphologies

5.2.2 Erosion Corrosion Behavior of API 5L X65 Carbon Steel

Figure 5.17 shows the impingement erosion corrosion rate of API 5L X65 carbon steel, as a function of impingement angle and velocity. With the introduction of solid particles, the overall trend remains the same as discussed in previous section. However there is significant increase in weight loss of material at all angles which is due to the influence of solid particles on impingement corrosion. However the mechanism involved in impingement erosion corrosion at angles i.e. 15° and 30° (Fig 5.18 a-b) indicated that there are elongated erosive tracks of ploughing, and micro cutting. It seems to be dominant over the indentation which is observed at higher angles after 45° degrees. These are more elongated ploughing tracks than that observed in case of AIS 1030 steel. This is expected because of more ductility in case of X65 steel. It is observed that there is more plastic deformation and raised lips, which contributed towards its better resistance to impingement erosion-corrosion by absorbing the stress energy due to little more ductility as compared to AISI 1030 carbon steel. At 45° (Fig 5.18 c) severe plastic deformation and deeper ploughed areas was found, together with more signs of surface activation due to expected balance between shear and normal impact stress. After 45° the shallower and shorter erosive tracks at an angle of 60° indicates the lesser effects of cutting. Wider tracks due to domination of normal impact stress, along with more frictional force for the particles to slide over the surface. At normal impingement angle i.e. 90º, particles strike the surface with their maximum kinetic energy and imparted the full normal impact stress. This resulted in flake formation and, platelets then their fracture, removal due to multiple subsequent strikes of the incoming particles Fig 5.18 (e). Furthermore the erosive tracks become wider and some micro cracks also found at high incidence angles.

Because of the slight increase in micro hardness value of the surface and work hardening [68]. After multiple strikes of the sand particles (i.e. 303Hv average value measured after experiment), there is slight increase in weight loss after 60º .

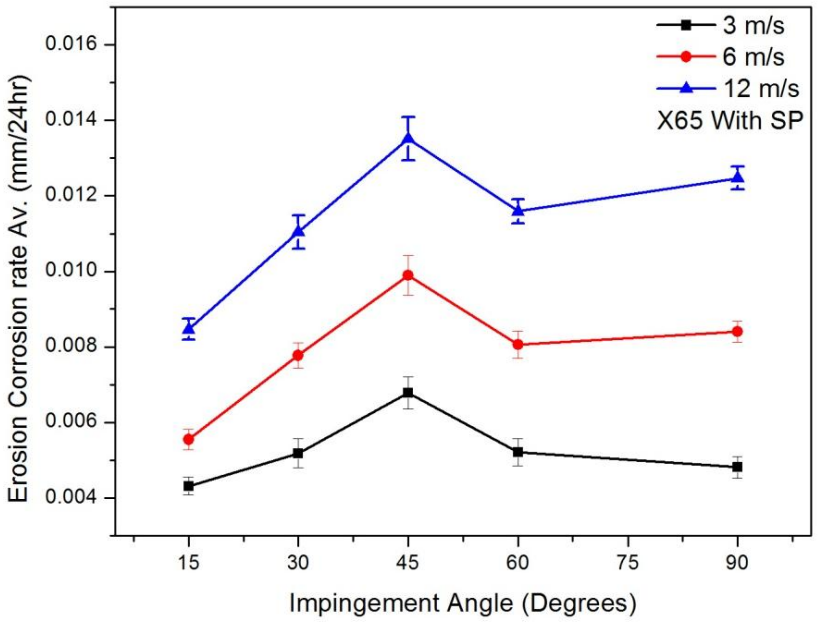

Figure 5.17 Impingement erosion corrosion rate as a function of angle and velocity.

Table 5. 5 Impingement Corrosion Rate as a Function of Angle and Velocity

Impingement Erosion Corrosion Rate, API X65 (Average, mm/24hr) With SP						
Impingement Angle		15	30	45	60	90
Jet Velocity	3m/s	0.0043	0.0051	0.0067	0.0052	0.0048
	6m/s	0.0055	0.0077	0.0098	0.0080	0.0084
	12m/s	0.0084	0.0110	0.0135	0.0115	0.0124

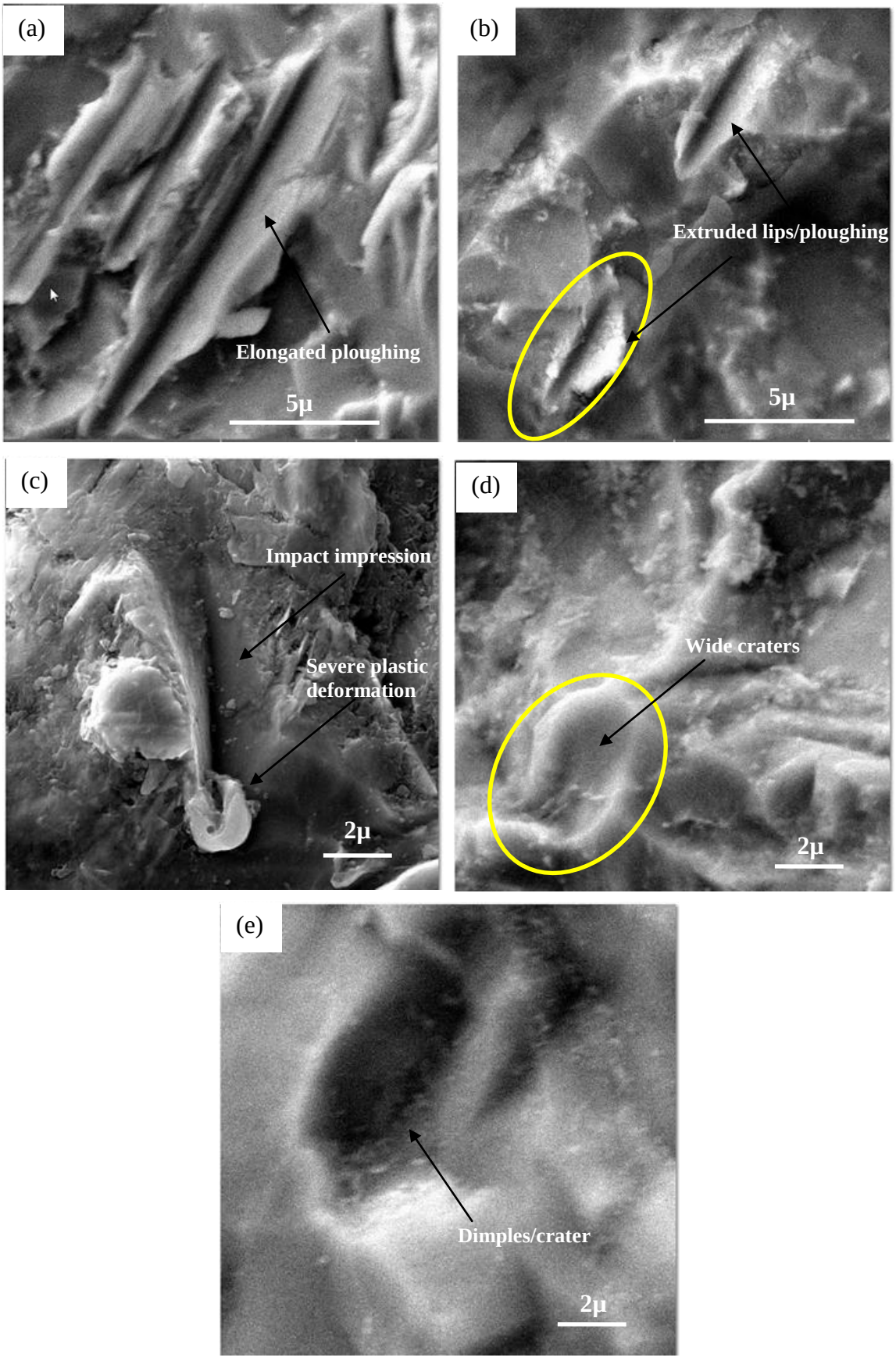

Figure 5. 18 FESEM images shows the erosion corrosion mechanism involves at various angles (a 15 to e 90 respectively).

5.2.3 Correlation with Erosion Corrosion Model

It is very useful to simulate to predict the erosion corrosion behavior of materials under consideration environment in the form of correlations. Prediction models are expressed generally as a function of velocity, impingement angle, particle size and shape, target material properties. Most famous models are those presented by Finnie [62, 63], Sundararajan [52] and hutching [51]. Model that is presented by Finnie and recently utilized by Xianghui Chen [64] at university of Tulsa erosion corrosion research group for carbon steel is as given below.

$$\mathrm{ER} = AF_s V^n f(\theta) \qquad \text{eq (2)}$$

Where ER is the erosion rate (mg/mg), A is an empirical constant, V is the particle impingement velocity, and n is an empirical coefficient. In research at erosion corrosion research centre of university of Tulsa demonstrated that a value of n is equal to 1.73 and that is fit to utilizing for various oilfield materials. F_s is a particle shape coefficient, Fs = 1.0 for angular sand particles. While f theta is the function of the impact angle that is given in below equation.

$$f(\theta) = x\cos^2\theta\sin(w\theta) + y\sin^2\theta + z \qquad \text{eq (3)}$$

Whereas w, x, y, and z are empirical constants that depend on the material being eroded. The suitable values of the model constants, assuming V has units of ft/s, are provided by

for carbon steel [64]. In the present work, the experimental data was correlated with above mentioned model and values of A and z were determined by performing regression analysis using MATLAB software. Lower and upper bounds for A are 0.012 and 0.0396 whereas for z are 0.428 and 0.572 respectively. Values of the correlation coefficient R2 > 99% indicating a good fit using the given parameters [64]. Furthermore, using known parameters mentioned above, erosion rates were calculated at v = 12 m/s for impingement angles ranging from 15° to 90°. A comparison between the experimental erosion rate curves with those calculated using Finnie model is shown in Figure7. The calculated erosion rate indicates a good agreement with the present experimental data of API 5L-X65 carbon steel. Consequently, the model of Finnie can be used to determine the erosion corrosion rate with reasonable accuracy. However, the parameters for this model given and calculated are specific to current test materials and test conditions.

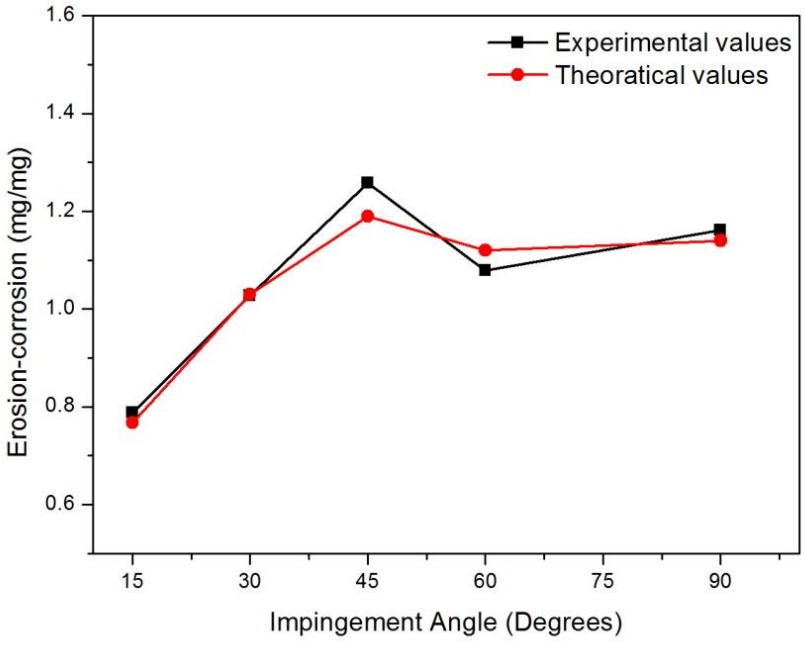

Figure 5.19 Comparison of experimental and Finnie et al. model curve fitting erosion-corrosion rate curves for carbon steel API 5L X65

5.2.4 Effect of Erosion on Corrosion

Figure 5.20 shows, that the impingement erosion corrosion has a considerable effect on material loss because of the effect of erosion on corrosion at all impingement angles. It was found that the introduction of solid particles increases the impingement erosion corrosion mechanism of API 5L X65 steel at all impingement angles as compared to impingement corrosion i.e. in the absence of solid particles. In case of X65 steel, it is clear from the graph (Fig 5.20) that the synergistic effect at 45° and 90° is more as compared to lower angles, which is similar trend that was found in case of 1030 steel. However in X65 we found that because of its ductility, ability to absorb energy in plastic deformation and work hardening, the synergistic effect is almost equal at these two angles (45º, 90º). This is because of balance between shearing stress, normal impact stress and deeper penetration at 45° resulted in surface activation and work hardening at 90° angle accelerates corrosion as shown in SEM images Fig 5.21. Furthermore at 90° impact angle due to extensive extrusion and fracture of platelets, erosion enhances corrosion considerably. We considered impingement corrosion rates as pure corrosion damage; however by introducing solid particles we have total damage of erosion and corrosion which we called impingement erosion-corrosion.

$$\text{Total Impigement EC} = \text{Impingement Corrosion} + \text{Impingement Erosion} \qquad \text{eq (4)}$$

Hence the synergistic effect or effect of erosion on corrosion is obtained by subtracting the impinging corrosion values from total material loss in results of impingement erosion corrosion by solid particles. We did EDX at 90º and 45º, and we found no evidence of the sand particles embedment in the surface Fig 5.22.

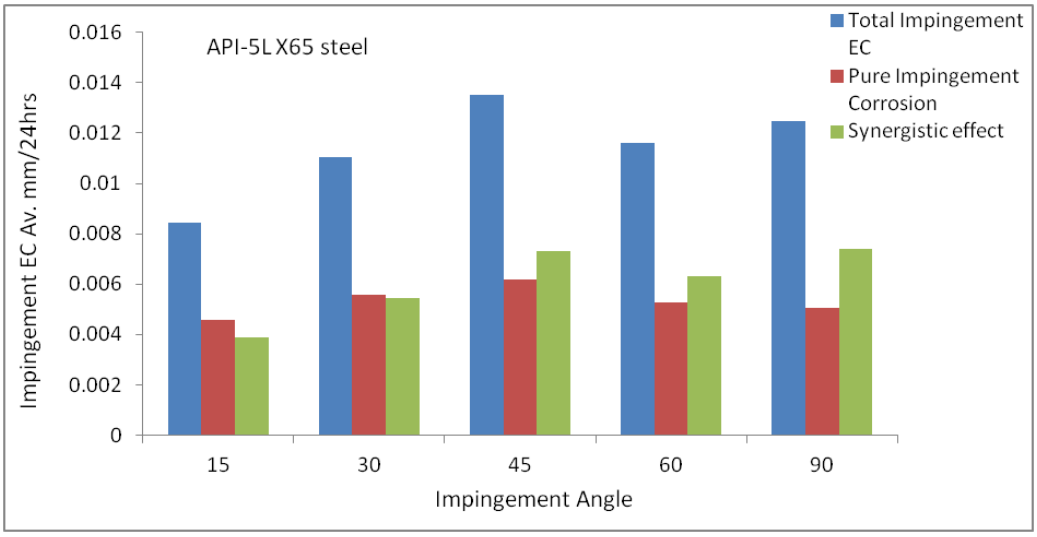

Figure 5.20 Effect of Impingement erosion on corrosion mass loss rate with the introduction of sand particles.

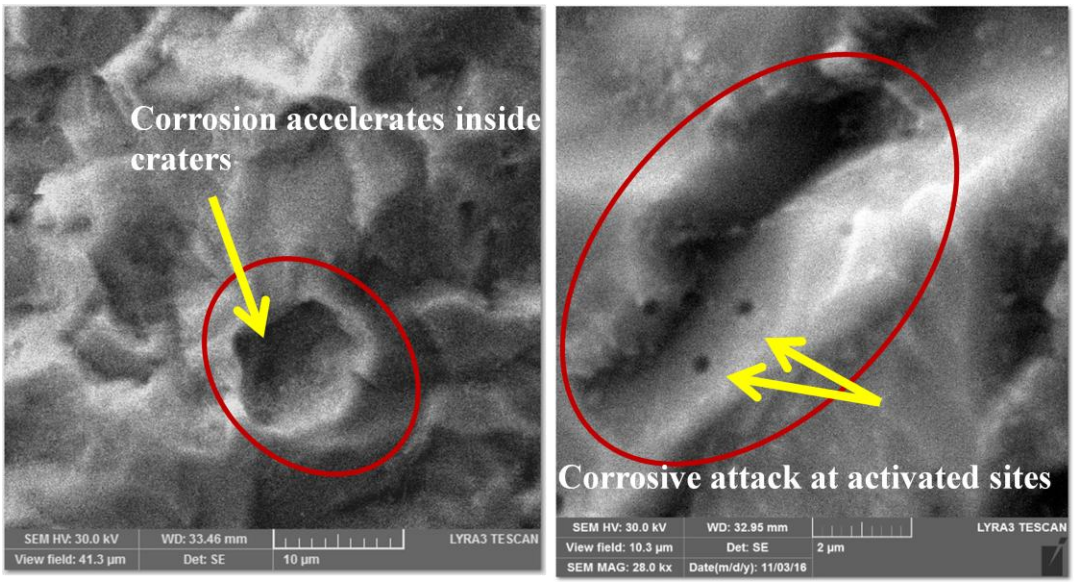

Figure 5. 21 Effects of Solid particle impingement on material loss.

(a)

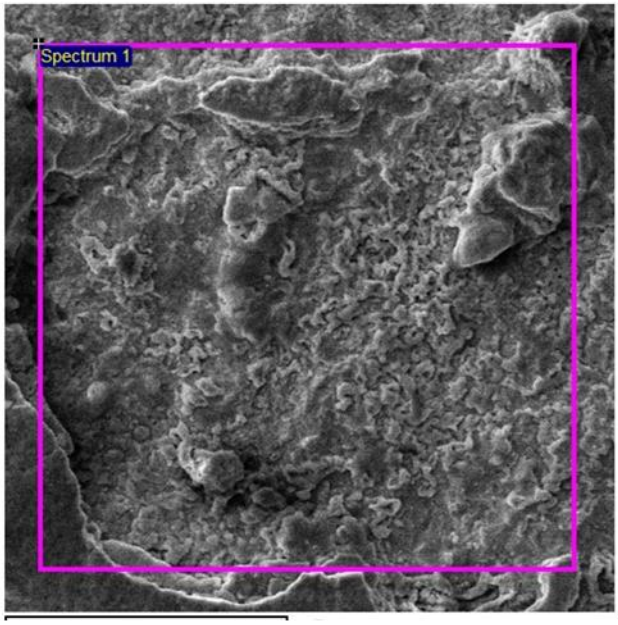

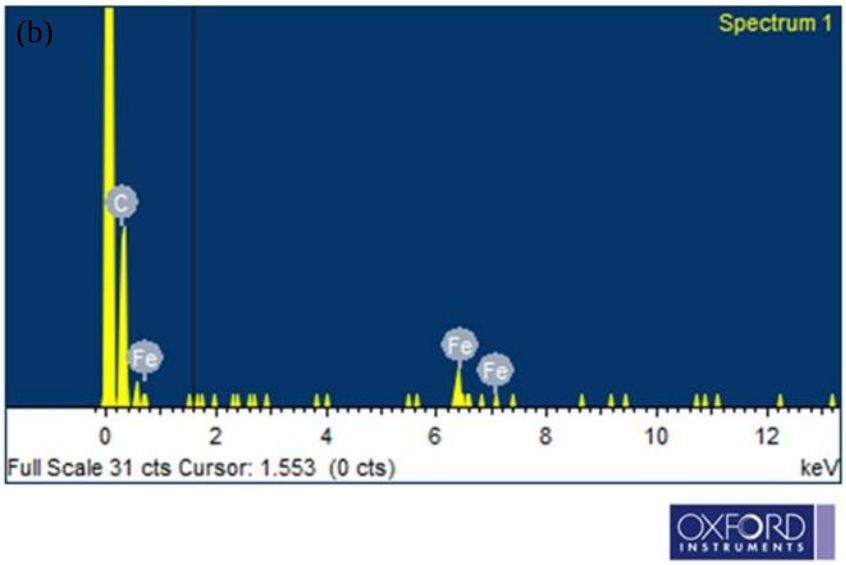

Figure 5.22 EDX Analysis of tested sample API 5L X65 Steel at 90º in presence of solid particles

5.2.5 Wear Scar Penetration Depths Using Optical Profilometer

At high velocity regions near the impingement point, we analyze the depth (average) of the wear scars that are produced after experimentation for 24 hrs at 15 to 90° angles and 12 m/s jet velocity. Typical 3D image analysis of wear scars and their penetration depths were examined and verified by A GTK-A 3D optical profiler from Bruker Co. Fig 5.23 shows the profile of region near impingement points, it is a function of impingement angle and the effect of solid particles on impingement corrosion. In case of X65 we found in impingement corrosion (without solid particles) as we increase the angle up to 45° degree the penetration depth becomes maximum i.e. 36 ± 5 µm, Table 5.6 (3D images shown in Fig 5.24). However, with solid particles it is clear that the particle ploughed deeper (as discussed in earlier sections) at intermediate angle i.e.45° degree giving 51 ± 5 µm depth. whereas at 90° angle particles strike with their maximum kinetic energy and activates the surface by extrusion, which resulted in platelet formation then these were fractured and removed by the subsequent impact of the particles. Hence as shown in Fig 5.25, the area exactly at impingement point also eroded and recessed scars were becomes wider. Maximum depth at 90° angle was 35 ± 3 µm in case of solid particles (table 5.6).

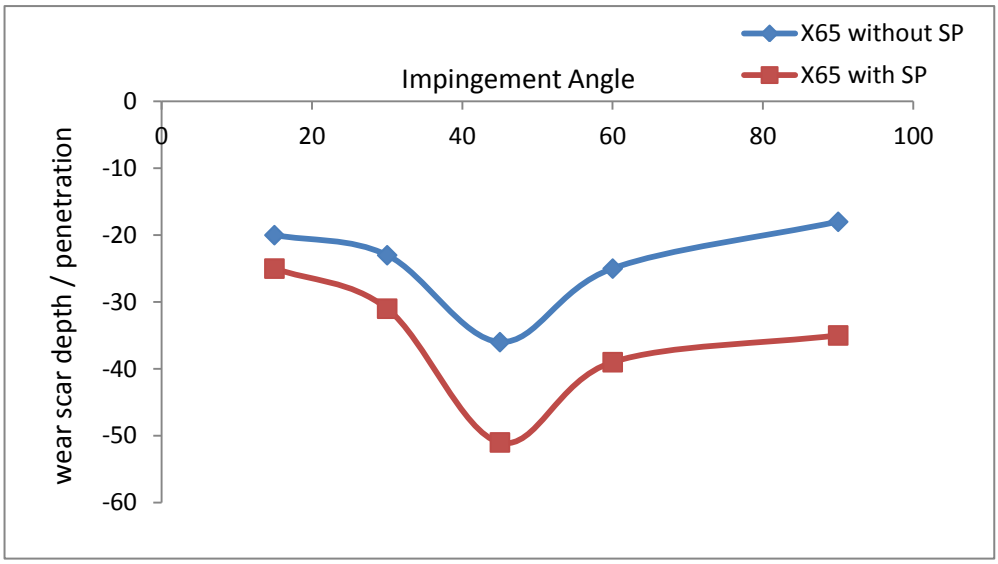

Figure 5. 23 Wear Scar Penetration depths X65 Steel

Table 5. 6 Average Scar Depth Values (API 5L X65 Steel)

Impingement Angle	15	30	45	60	90
Wear Scar Depth (µm) X65 without SP	20	23	36	25	18
Wear Scar Depth (µm) X65 with SP	25	31	51	39	35

(a) 15°

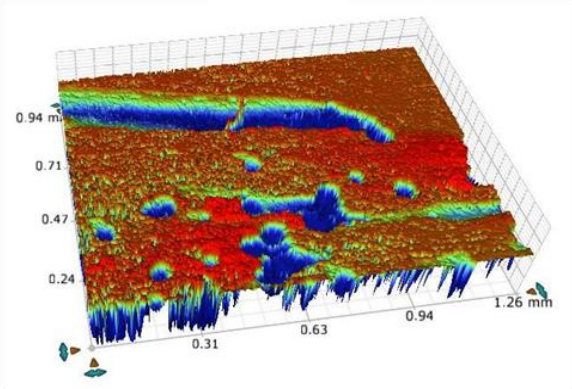

(b) 30°

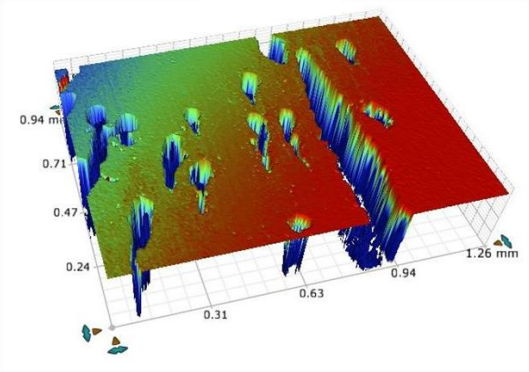

(c) 45°

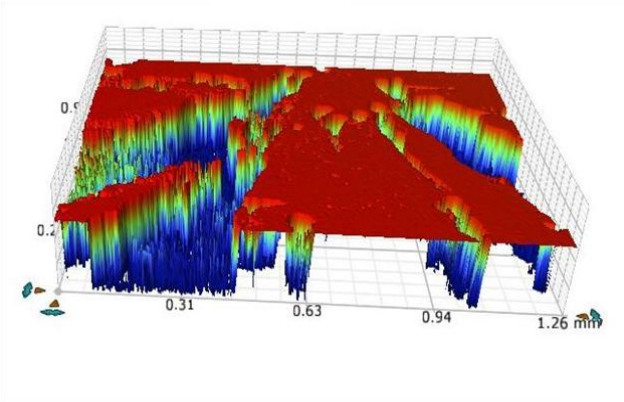

(d) 60°

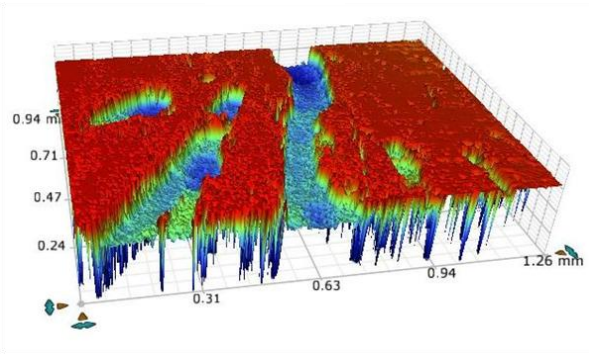

(e) 90°

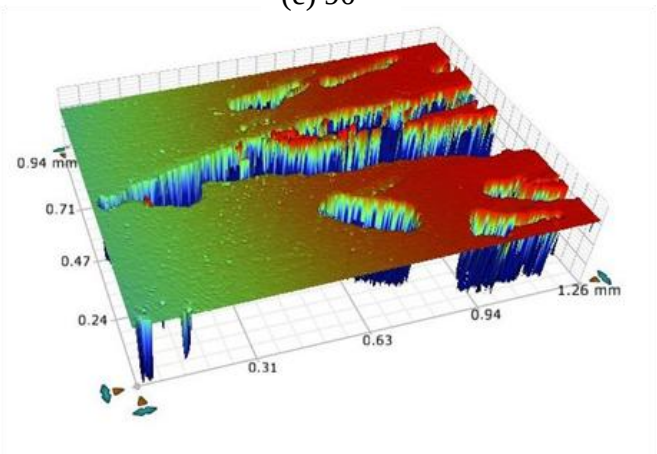

Figure 5.24 Optical images near high velocity regions in absence of particles

(a) 15°

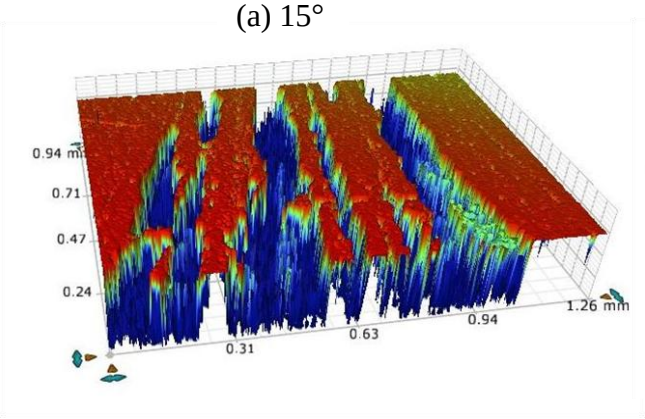

(b) 30°

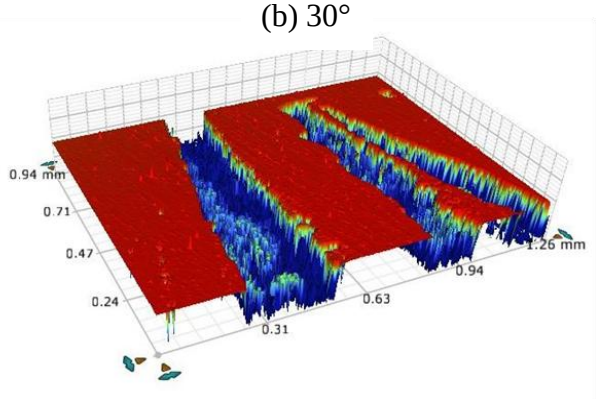

(c) 45°

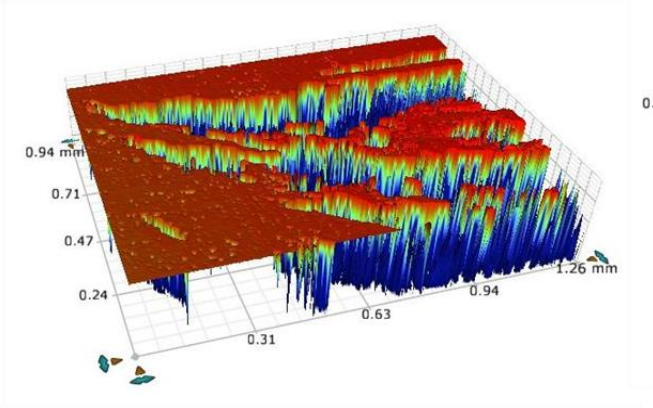

(d) 60°

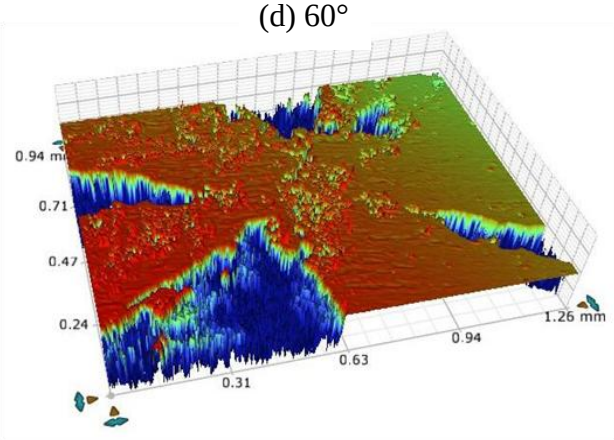

(e) 90°

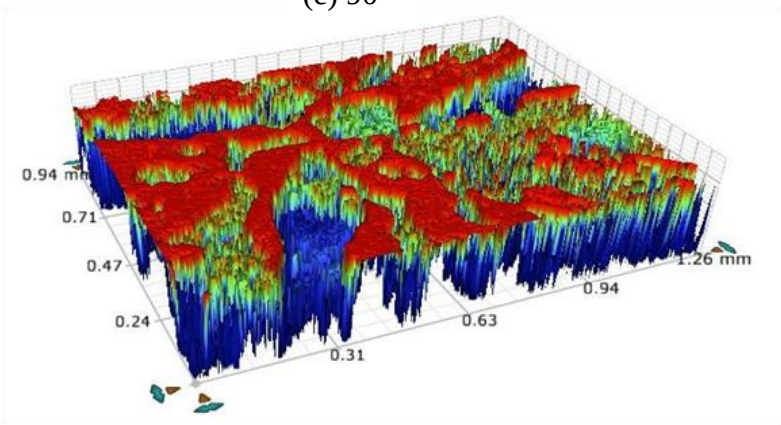

Figure 5. 25 Optical images near high velocity regions in presence of solid particles

CHAPTER 6

CONCLUSIONS AND FUTURE RECOMMENDATIONS

6.1 Conclusions

An experimental study was performed using multi purpose Flowloop to investigate the impingement corrosion and erosion corrosion of AISI 1030 and API 5L X65 steels in low saline fluid in the absence of solid particles and in the presence of silica sand particles (Average particle size of 314 µm). Impingement corrosion and erosion corrosion measurements were conducted for five different impingement angles i.e. 15°, 30°, 45°, 60° and 90°, using three different jet velocities i.e. 3 m/s, 6m/s and 12 m/s at each angle. Finally wear scars were examined to understand the depth morphology under such conditions. Based on the obtained results, following conclusions can be drawn.

1) API 5L X65 steel exhibit better impingement corrosion and erosion corrosion resistance as compared to AISI 1030 steel because of its higher ductility and low hardness.

2) At low impingement angles, ploughing, elongated erosive tracks, and metal cutting were the dominating erosion corrosion mechanisms. Whereas, at higher impingement angles, extrusion, flattening of ridges and fracture was the dominant process of material removal.

3) Impingement corrosion and erosion corrosion rate increases with an increase in jet velocity in both type of steels. Increase in velocity increases the shear and normal impact stresses which resulted in more mass loss.

4) The maximum impingement corroison and erosion corrosion rates were found at 45°, at this angle there is a balance between shearing stress and normal impact stress. Secondly in presence of solid particles there was deep pentration of the particles in to the target material which was resposible for the more demage.

5) Solid particles have significant effects on corrosion as particles impinged and cut the surafce and activate the localised sites, this resulted into accelerates the impingement corrosion rate.

6) No protective oxide layer due to impingement at such high velocity conditions. The oxide layer continuously removed by fluid flow and due to the impact of solid particles.

6.2 FUTURE RECOMMENDATIONS

1) Online monitoring for various conditions (impingement velocity, angles and fluid compositions).

2) Impingement Erosion Corrosion for different type of metals (Aluminium, Stainless steels, Copper alloys).

3) Investigation on solid particle size effect and their concentration.

4) Study the effect of Inhibitors on erosion corrosion rate and mechanism involved.

REFERENCES

[1] Fontana, M.G., *Corrosion engineering*. 2005: Tata McGraw-Hill Education.

[2] Levy, A.V., *Solid particle erosion and erosion-corrosion of materials*. 1995: Asm International.

[3] Heidersbach, R., *Metallurgy and corrosion control in oil and gas production*. Vol. 14. 2010: John Wiley & Sons.

[4] Javaherdashti, R., C. Nwaoha, and H. Tan, *Corrosion and materials in the oil and gas industries*. 2013: CRC Press.

[5] Neville, A., M. Reyes, and H. Xu, *Examining corrosion effects and corrosion/erosion interactions on metallic materials in aqueous slurries.* Tribology International, 2002. **35**(10): p. 643-650.

[6] Mazumder, Q.H., *Prediction of Erosion due to solid particle Impact in Single-Phase and Multiphase Flows.* Journal of Pressure Vessel Technology, 2007. **129**(4): p. 576-582.

[7] Efird, K., et al., *Correlation of steel corrosion in pipe flow with jet impingement and rotating cylinder tests.* Corrosion, 1993. **49**(12): p. 992-1003.

[8] Efird, K.D. *Flow accelerated corrosion testing basics*. in *CORROSION 2006*. 2006. NACE International.

[9] Giourntas, L., T. Hodgkiess, and A. Galloway, *Enhanced approach of assessing the corrosive wear of engineering materials under impingement.* Wear, 2015. **338**: p. 155-163.

[10] Sasaki, K. and G. Burstein, *Erosion–corrosion of stainless steel under impingement by a fluid jet.* Corrosion science, 2007. **49**(1): p. 92-102.

[11] Khan, M.I. and T. Yasmin, *Erosion–Corrosion of Low Carbon (AISI 1008 Steel) Ring Gasket Under Dynamic High Pressure CO2 Environment.* Journal of Failure Analysis and Prevention, 2014. **14**(4): p. 537-548.

[12] Barker, R., et al. *Flow-induced corrosion and erosion-corrosion assessment of carbon steel pipework in oil and gas production*. in *CORROSION 2011*. 2011. NACE International.

[13] Neville, A., T. Hodgkiess, and J. Dallas, *A study of the erosion-corrosion behaviour of engineering steels for marine pumping applications.* Wear, 1995. **186**: p. 497-507.

[14] Salama, M.M. *Influence of sand production on design and operations of piping systems*. in *CORROSION 2000*. 2000. NACE International.

[15] Finnie, I., *Erosion of surfaces by solid particles.* Wear, 1960. **3**(2): p. 87-103.

[16] Sundararajan, G. and M. Roy, *Solid particle erosion behaviour of metallic materials at room and elevated temperatures.* Tribology International, 1997. **30**(5): p. 339-359.

[17] Matsumura, M., et al., *The role of passivating film in preventing slurry erosion-corrosion of austenitic stainless steel.* ISIJ international, 1991. **31**(2): p. 168-176.

[18] Zu, J., G. Burstein, and I. Hutchings, *A comparative study of the slurry erosion and free-fall particle erosion of aluminium.* Wear, 1991. **149**(1): p. 73-84.

[19] Fuyan, L. and S. Hesheng, *The effect of impingement angle on slurry erosion.* Wear, 1991. **141**(2): p. 279-289.

[20] Islam, M.A., et al., *Erosion enhanced corrosion and corrosion enhanced erosion of API X-70 pipeline steel.* Wear, 2013. **302**(1): p. 1592-1601.

[21] Akbarzadeh, E., et al., *The solid particle erosion of 12 metals using magnetite erodent.* Wear, 2012. **282**: p. 40-51.

[22] Mohammadi, F., *Erosion-corrosion of 304 Stainless Steel*, 2011, University of Alberta.

[23] McMahon, A.J., J.W. Martin, and L. Harris. *Effects of sand and interfacial adsorption loss on corrosion inhibitor efficiency*. in *CORROSION 2005*. 2005. NACE International.

[24] Neville, A. and C. Wang, *Erosion–corrosion mitigation by corrosion inhibitors—an assessment of mechanisms.* Wear, 2009. **267**(1): p. 195-203.

[25] Tilly, G., *Erosion caused by airborne particles.* Wear, 1969. **14**(1): p. 63-79.

[26] Finnie, I., *Some observations on the erosion of ductile metals.* wear, 1972. **19**(1): p. 81-90.

[27] Levy, A., *Erosion and erosion-corrosion of metals.* Corrosion, 1995. **51**(11): p. 872-883.

[28] Levy, A., M. Aghazadeh, and G. Hickey, *The effect of test variables on the platelet mechanism of erosion.* Wear, 1986. **108**(1): p. 23-41.

[29] Adler, T.A. and Ö.N. Doğan, *Erosive wear and impact damage of high-chromium white cast irons.* Wear, 1999. **225**: p. 174-180.

[30] Chen, Q. and D. Li, *Computer simulation of solid particle erosion.* Wear, 2003. **254**(3): p. 203-210.

[31] Evans, A. and T.R. Wilshaw, *Quasi-static solid particle damage in brittle solids—I. Observations analysis and implications.* Acta Metallurgica, 1976. **24**(10): p. 939-956.

[32] Neville, A., et al., *Erosion–corrosion behaviour of WC-based MMCs in liquid–solid slurries.* Wear, 2005. **259**(1): p. 181-195.

[33] Madsen, B.W., *Measurement of erosion-corrosion synergism with a slurry wear test apparatus.* Wear, 1988. **123**(2): p. 127-142.

[34] Li, Y., G. Burstein, and I. Hutchings, *The influence of corrosion on the erosion of aluminium by aqueous silica slurries.* Wear, 1995. **186**: p. 515-522.

[35] Lu, B., et al. *Effects Of Slurry Ph On The Surface Mechanical Properties And Erosion-Corrosion Resistance*. in *CORROSION 2008*. 2008. NACE International.

[36] Zheng, Y., et al., *The synergistic effect between erosion and corrosion in acidic slurry medium.* Wear, 1995. **186**: p. 555-561.

[37] Heidemeyer, J., *Influence of the plastic deformation of metals during mixed friction on their chemical reaction rate.* Wear, 1981. **66**(3): p. 379-387.

[38] Burstein, G. and K. Sasaki, *Effect of impact angle on the slurry erosion–corrosion of 304L stainless steel.* Wear, 2000. **240**(1): p. 80-94.

[39] Neville, A. and C. Wang, *Erosion–corrosion of engineering steels—Can it be managed by use of chemicals?* Wear, 2009. **267**(11): p. 2018-2026.

[40] Mansouri, A., et al., *A combined CFD/experimental methodology for erosion prediction.* Wear, 2015. **332**: p. 1090-1097.

[41] Clark, H.M., *The influence of the flow field in slurry erosion.* Wear, 1992. **152**(2): p. 223-240.

[42] Sundararajan, G., *The differential effect of the hardness of metallic materials on their erosion and abrasion resistance.* Wear, 1993. **162**: p. 773-781.

[43] Abbade, N.P. and S.J. Crnkovic, *Sand–water slurry erosion of API 5L X65 pipe steel as quenched from intercritical temperature.* Tribology International, 2000. **33**(12): p. 811-816.

[44] Zu, J., I. Hutchings, and G. Burstein, *Design of a slurry erosion test rig.* Wear, 1990. **140**(2): p. 331-344.

[45] Wentzel, E.J. and C. Allen, *Erosion-corrosion resistance of tungsten carbide hard metals with different binder compositions.* Wear, 1995. **181**: p. 63-69.

[46] Levy, A. and G. Hickey, *Liquid-solid particle slurry erosion of steels.* Wear, 1987. **117**(2): p. 129-146.

[47] Malik, J., et al., *Evaluating the Effect of Hardness on Erosion Characteristics of Aluminum and Steels.* Journal of Materials Engineering and Performance, 2014. **23**(6): p. 2274-2282.

[48] Levy, A.V. and P. Yau, *Erosion of steels in liquid slurries.* Wear, 1984. **98**: p. 163-182.

[49] Nava, J.C., F. Stott, and M. Stack, *The effect of substrate hardness on the erosion-corrosion resistance of materials in low-velocity conditions.* Corrosion science, 1993. **35**(5-8): p. 1045-1051.

[50] Pasha, A., H. Ghasemi, and J. Neshati, *Synergistic erosion-corrosion behavior of X-65 carbon steel at various impingement angles.* Journal of Tribology, 2016.

[51] Hutchings, I., *A model for the erosion of metals by spherical particles at normal incidence.* Wear, 1981. **70**(3): p. 269-281.

[52] Sundararajan, G. and P. Shewmon, *A new model for the erosion of metals at normal incidence.* Wear, 1983. **84**(2): p. 237-258.

[53] Bitter, J., *A study of erosion phenomena part I.* wear, 1963. **6**(1): p. 5-21.

[54] Levy, A.V. and P. Chik, *The effects of erodent composition and shape on the erosion of steel.* Wear, 1983. **89**(2): p. 151-162.

[55] ASTM Standard, G.-. *Liquid Impingement Erosion Testing1*. 1998. **Vol 08.01**.

[56] 03, A.S.G., *Standard Practice for Preparing, Cleaning, and Evaluating Corrosion Test Specimens.* 2003. **Vol 01.03**.

[57] Liang, G., et al., *Erosion-corrosion of carbon steel pipes in oil sands slurry studied by weight-loss testing and CFD simulation.* Journal of materials engineering and performance, 2013. **22**(10): p. 3043-3048.

[58] Lin, F. and H. Shao, *Effect of impact velocity on slurry erosion and a new design of a slurry erosion tester.* Wear, 1991. **143**(2): p. 231-240.

[59] Jingjun, L., L. Yuzhen, and L. Xiaoyu, *Numerical simulation for carbon steel flow-induced corrosion in high-velocity flow seawater.* Anti-Corrosion Methods and Materials, 2008. **55**(2): p. 66-72.

[60] Islam, M.A., et al., *Effect of microstructure on the erosion behavior of carbon steel.* Wear, 2015. **332**: p. 1080-1089.

[61] Abedini, M. and H. Ghasemi, *Synergistic erosion–corrosion behavior of Al–brass alloy at various impingement angles.* Wear, 2014. **319**(1): p. 49-55.

[62] Finnie, I. and Y. Kabil, *On the formation of surface ripples during erosion.* Wear, 1965. **8**(1): p. 60-69.

[63] Wong, C.Y., et al., *Predicting the material loss around a hole due to sand erosion.* Wear, 2012. **276**: p. 1-15.

[64] Chen, X., B.S. McLaury, and S.A. Shirazi, *Application and experimental validation of a computational fluid dynamics (CFD)-based erosion prediction model in elbows and plugged tees.* Computers & Fluids, 2004. **33**(10): p. 1251-1272.

[65] Ige, O. and L. Umoru, *Effects of shear stress on the erosion-corrosion behaviour of X-65 carbon steel: A combined mass-loss and profilometry study.* Tribology International, 2016. **94**: p. 155-164.

[66] Nguyen, Q., et al., *Effect of impact angle and testing time on erosion of stainless steel at higher velocities.* Wear, 2014. **321**: p. 87-93.

[67] Guanghong, Z., et al., *Corrosion–erosion wear behaviors of 13Cr24Mn0. 44N stainless steel in saline–sand slurry.* Tribology International, 2010. **43**(5): p. 891-896.

[68] Lin, H., S. Wu, and C. Yeh, *A comparison of slurry erosion characteristics of TiNi shape memory alloys and SUS304 stainless steel.* Wear, 2001. **249**(7): p. 557-565.

VITAE

Name	:Hafiz Muzammil Irshad
Nationality	:Pakistan
Date of Birth	:8/12/1986
Email	:Muzammil.duke@gmail.com
Address	:362A1-PGECHS, Lahore Pakistan
Academic Background	: MS Materials Science & Engineering, KFUPM Dhahran, Saudi Arabia
	BS Metallurgy & Materials Engineering, University of the Punjab Lahore, Pakistan.

Participations:

- 16th Middle East Corrosion Conference, 2016 Bahrain
  (Poster presentation)

  Title: Study the effect of velocity and angle on Impingement erosion-corrosion behaviour of Carbon steel AISI 1030

- Speaker at 5th Corrosion Management Summit 2016, Khober

  Title: Experimental Investigations of the Erosion & Corrosion-Enhanced Erosion Phenomenon in Different Metals

Publications:

- Solid Particle Erosion Behavior of Glass Fiber Reinforced Polyester and Epoxy Resin Composites. (Submitted)
- Liquid Impingement Corrosion behavior of AISI 1030 mild Steel under low saline fluid jet in a Flowloop. (Submitted)
- Effect of velocity and impact angle of fluid jet on the erosion corrosion behavior of X65 carbon steel. (Submitted)